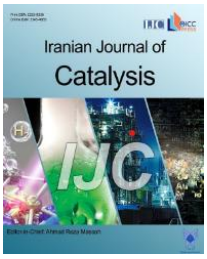

Iran. J. Catal. 2026; 16(1): 80-100

Iranian Journal of Catalysis (IJC)

https://doi.org/10.57647/ijc.2026.1601.06

Research Article

Functionalizing Fullerene Soot Nanoparticles with Energetic Groups Using Copper-Catalyzed Oxidative Deboration of Nitrophenylboronic Acid

Fatemeh Sadat Hosseini, Mehdi Zamani*

School of Chemistry, Damghan University, Damghan, Iran

*Corresponding authors: m.zamani@du.ac.ir

Article History:

Received:
17June 2025

Revised:
22 October 2025

Accepted:
10 November 2025

Published Online:
25 November 2025

Published in Issue:
31 March 2026

Abstract

In this study, 4-nitrophenylboronic acid is used as a radical precursor for functionalizing fullerene soot nanoparticles with 4-nitrophenyl and 4-nitrophenoxy groups. The oxidative deboration of 4-nitrophenylboronic acid for the formation of 4-nitrophenyl radical is carried out by employing potassium persulfate as oxidant and copper (II) sulfate as catalyst dissolved in water/dichloromethane under autoclave, oil-bath, or microwave heating conditions. The 4-nitrophenoxy radical is formed from the corresponding phenolic byproduct in the presence of persulfate/copper (II). The potentially energetic solid containing 4-nitrophenoxy groups involved in ether linkages is produced in the absence of fullerene soot. The 4-nitrophenyl and 4-nitrophenoxy radicals are efficiently trapped in the presence of fullerene soot to eventually afford samples with high nitrogen contents. The reaction conditions are optimized against temperature, time, and the amounts of starting materials. The characterization of products is performed by EDX and elemental maps, FT-IR, XRD, FESEM, and TGA-DSC. Results show that the oxidative deboration reaction can occur even in the absence of a catalyst. However, copper (II) catalyst can be used to obtain samples with more nitrogen content (up to 19.60 wt.% by EDX line scan) and better energetic performance. DSC thermograms of these samples exhibit a significant exothermic peak assigned to the decomposition of energetic groups.

Keywords: Arylboronic acid; Aryl and aryloxy radicals; Energetic groups; Fullerene soot nanoparticles; Oxidative deboration; Persulfate/copper (II)

Cite this article: F. S. Hosseini, M. Zamani, Iran. J. Catal. **16** (2026) 80-100. https://doi.org/10.57647/ijc.2026.1601.06

1. Introduction

The preparation of high-energy compositions based on carbon nanomaterials has recently attracted considerable attention, because using carbon nanomaterials in energetic compositions would greatly improve their combustion performance, thermal stability, and sensitivity [1]. Graphene, graphene oxide, carbon nanotubes, and fullerene have been introduced to prepare core-shell structured explosives due to their unique electrical, thermal, mechanical, and structural properties [2]. These carbon materials can be utilized to desensitize the explosives significantly with a low additive amount [2]. Also, due to their large surface areas, they have demonstrated promising results as burn rate modifiers for propellants [3].

Fullerenes and their derivatives are important for applications in energetic materials, which are used as energetic components, combustion catalysts, desensitizers, and stabilizers [4]. They show good thermal performance as energetic components [4]. They can reduce the activation energy of energetic materials as

combustion catalysts [4]. They can reduce the friction sensitivity and impact sensitivity of explosives as desensitizers [4]. They have a high scavenging rate of nitrogen oxide radicals as stabilizers [4]. Also, C_{60}, due to the large mass, low first ionization potential, and large electron impact ionization cross-section, has the potential for significant increases in engine efficiency as an ion engine propellant [5].

The addition of fullerene and fullerene soot additives to nitroglycerine as an important ingredient of dynamite markedly accelerates its liquid phase decomposition [6]. Also, the solid phase decomposition of nitrocellulose and the liquid phase decomposition of RDX are accelerated by the addition of fullerene soot [6]. Fullerene and fullerene soot additives can improve the burning rate and promote the combustion efficiency of RDX composite modified double-base (RDX-CMDB) propellants [7-9].

By incorporating the fullerene derivatives, the burn rate of the ammonium perchlorate-based propellants increases, accompanied by a rise in their calorific value [3,10,11]. The use of fullerene soot in the ammonium nitrate-based propellants can provide an increase in burning rate [12]. Fullerene-based lead salt has potential application as a combustion catalyst in solid propellant [13]. The fullerene hydrazine nitrate, as a new potential energetic combustion catalyst, can accelerate the decomposition of RDX and HMX [14]. The polynitrofullerene has been introduced as buckybomb, which can be used to design novel energetic materials [15]. The polyaminofullerene nitrate with high nitrogen content has potential application in explosives and propellant additives [16].

It has been reported that carbon nanomaterials become energetic when decorated with one or more nitroaromatic substituents [17-22]. Addition of nitroaryl groups (NO_2Ar–) to these compounds increases their energy density and enhances their energy-releasing properties [17-22]. The $–NO_2$ substituted aryl radicals ($NO_2Ar^{\bullet}$) have been generally used to functionalize carbon nanomaterials [17-27].

The currently used aryl radical precursors include nitroaryl diazoniums ($NO_2ArN_2^+X^-$) [17,19,24,25], nitroaryl carboxylic acids (NO_2ArCO_2H) [21,22,26], and nitroaryl carboxylates ($NO_2ArCO_2^-M^+$) [27]. The purpose of the current study involves the development of a new synthetic method for functionalizing fullerene soot nanoparticles with energetic groups using nitroaryl boronic acids ($NO_2ArB(OH)_2$) as radical precursors. Boronic acids can be considered as safe and environmentally friendly compounds [28] compared to diazonium salts, which are hazardous [29].

To avoid the handling of hazardous compounds, nitroaryl diazonium salts are generated in situ from amine precursors and further react without isolation [30,31]. While nitroaryl boronic acids are chemically stable under standard ambient conditions and can be stored as dry when tightly closed or under inert gas [32].

Fullerenes, due to the highly π-conjugated system, and their soot analogues are known to behave like a radical sponge [33-35]. They have scavenging capacity towards carbon- and oxygen-centered radicals [36-43]. Fullerene soot is a carbonaceous material that contains fullerenes and carbon blacks [44]. The nanoparticles of fullerene soot are onion-like, curved graphitic layers that contain voids and defects [45]. The bonds at the edges of the defects, so-called dangling bonds, are usually free radical [45]. The fullerene moiety of the fullerene soot acts as a carbon-centered radical scavenger while the non-fullerene part operates as an oxygen-centered radical scavenger [36]. The radical scavenging activity of fullerene soot is higher than that of fullerenes, especially after the treatment with oxidants [36,37].

Arylboronic acids are one of the main sources of aryl radicals [46-48]. These compounds generate aryl radicals under oxidative conditions [46]. The aryl couplings proceed efficiently with arylboronic acids [49-56], even on the multi-layer graphitic materials [57] and carbon nanotubes [58]. 4-Nitrophenylboronic acid is a solid acid with the pK_a of 7.15 [59] that is generally used as a reagent in a variety of metal-catalyzed cross-couplings [60]. Recent advances in the radical reactions involving the nitro group have been reviewed [61]. The hydroxylation of arylboronic acids is a useful alternative pathway to phenol synthesis [62-64]. Potassium persulfate is an oxidant used for radical arylation [46]. Copper (II) is one of the most active catalysts used for oxidative coupling of organoboron compounds [65]. Copper/persulfate is an interesting coupling system due to its versatile activation pathways with the formation of multiple radical and nonradical species [66]. Other catalysts may be used instead of copper(II) for such oxidative coupling reactions, such as salts of manganese(III), silver(I), iron(II or III), nickel(II), bismuth(III), and palladium(II) [48,65].

In this study, we report a new process for functionalizing fullerene soot nanoparticles with energetic groups using copper-catalyzed oxidative deboration of 4-nitrophenylboronic acid (4-nitrophenylboronic acid as radical precursor, potassium persulfate as oxidant, and copper (II) sulfate as catalyst dissolved in water/dichloromethane) under autoclave, oil-bath, or microwave heating.

The reaction conditions are optimized against temperature, time, and the amounts of starting materials. The characterization of products is performed by energy-dispersive X-ray spectroscopy (EDX) line scan and elemental maps, Fourier transform infrared spectroscopy (FT-IR), X-ray diffraction (XRD) measurements, field emission scanning electron microscopy (FESEM), thermogravimetry analysis (TGA), and differential scanning calorimetry (DSC).

10.57647/ijc.2026.1601.06

2. Experimental section

2.1. Materials and instruments

Fullerene soot nanoparticles with fullerene content ≥ 5.0 % and 4-nitrophenylboronic acid (4-NO_2PhB $(OH)_2$) were purchased from Sigma-Aldrich. Potassium persulfate ($K_2S_2O_8$), copper (II) sulfate ($CuSO_4$), and dichloromethane (CH_2Cl_2) were purchased from Merck Chemical Co.

The TESCAN MIRA III Field Emission Microscope was used for EDX line scan and elemental maps, as well as FESEM analysis. The Thermo Nicolet 6700 Fourier transform infrared spectrophotometer was used to record FT-IR spectra in the range of 400-3500 cm^{-1} using KBr pellets. The Bruker D8-Advance X-ray diffractometer with CuKα radiation was used for XRD measurements in a 2θ range of 5-80°. The TA Q600 thermal analyzer instrument was used for TGA-DSC analysis in an air atmosphere in a range of 25-850 °C with a heating rate of 10 °C/min.

2.2. Functionalizing fullerene soot nanoparticles under autoclave heating

Initially, a fixed amount of fullerene soot (15 mg) and various amounts of the starting materials with different equivalent (equiv.) ratios of reactant, oxidant, and catalyst (0:3:0.2, 1:3:0.2, 1:3:0, 1:3:1, and 1:1:0.2) were weighed (Table 1). Then, the mixture of fullerene soot and reactant (4-nitrophenylboronic acid) in 5 mL of dichloromethane solvent was added to the solution of oxidant (potassium persulfate) and catalyst (copper(II) sulfate) in 5 mL of deionized water under stirring conditions. The resulting mixture was transferred to a 30 mL PTFE-lined stainless-steel autoclave and then heated with a hot plate at 60 °C or 120 °C under stirring for 1, 6, or 12 hours (Fig. 1). After cooling (aging time 12 h), the obtained solid sample was separated from the solution by centrifugation, washed with solvents, and centrifuged again. The final product was collected after air-drying on a glass plate.

2.3. Functionalizing fullerene soot nanoparticles under oil-bath heating

Initially, a fixed amount of fullerene soot (15 mg) and various amounts of the starting materials with different equivalents. Ratios of reactant, oxidant, and catalyst (1:3:0 and 1:3:0.2) were weighed (Table 1). Then, the mixture of fullerene soot and reactant (4-nitrophenylboronic acid) in 5 mL of dichloromethane solvent was added to the solution of oxidant (potassium persulfate) and catalyst (copper(II) sulfate) in 5 mL of deionized water under stirrer conditions. The resulting mixture was transferred to a 25 mL glass flask equipped with a reflux condenser and then heated in an oil bath with a stirrer/hot plate under reflux conditions for 6 or 12 hours, where the oil bath temperature was set at 60 or 120 °C (Figure 1). After cooling (immediately), the obtained solid sample was separated from the solution by centrifugation, washed with solvents, and centrifuged again. The final product was collected after air-drying on a glass plate.

2.4. Functionalizing fullerene soot nanoparticles under microwave heating

Initially, a fixed amount of fullerene soot (15 mg) and various amounts of the starting materials with different equivalents. ratios of reactant, oxidant, and catalyst (1:3:0 and 1:3:0.2) were weighed (Table 1). Then, the mixture of fullerene soot and reactant (4-nitrophenylboronic acid) in 5 mL of dichloromethane solvent was added to the solution of oxidant (potassium persulfate) and catalyst (copper (II) sulfate) in 5 mL of deionized water under stirrer conditions. The resulting mixture was transferred to a 25 mL glass cup sealed with aluminum foil and then heated in a microwave oven for 0.5 hour, where the power was set at 100 W (Fig. 1). After cooling (immediately), the obtained solid sample was washed with solvents and centrifuged. The final product was collected after air-drying on a glass plate.

3. Results and Discussion

3.1. Proposed mechanism for functionalizing fullerene soot nanoparticles

Experimental conditions used in this study for functionalizing fullerene soot nanoparticles with energetic groups using copper-catalyzed oxidative deboration of nitrophenylboronic acid are indicated in Fig. 1. Here, 4-nitrophenylboronic acid (reactant), potassium persulfate (oxidant), and copper(II) sulfate (catalyst) in water/dichloromethane (solvent) are selected as starting materials for functionalizing fullerene soot nanoparticles with 4-nitrophenyl (4-NO_2Ph–) and 4-nitrophenoxy (4-NO_2PhO–) groups under autoclave, oil-bath, or microwave heating conditions.

The aryl (Ar–) and aryloxy (ArO–) groups (Ar = 4-NO_2Ph) can be obtained from the corresponding arylboronic acid ($ArB(OH)_2$) as radical precursor. In the proposed mechanism (Fig. 2), under high temperature [67] or microwave irradiation [68], persulfate ion ($S_2O_8^{2-}$) is converted to a powerful oxidant known as the sulfate radical anion ($SO_4^{\bullet-}$), which initiates the formation of aryl radical ($Ar^{\bullet}$) from arylboronic acid. The aryl radical formation occurs either directly at the phase boundary or in the aqueous phase through diffusion of arylboronic acid [69].

10.57647/ijc.2026.1601.06

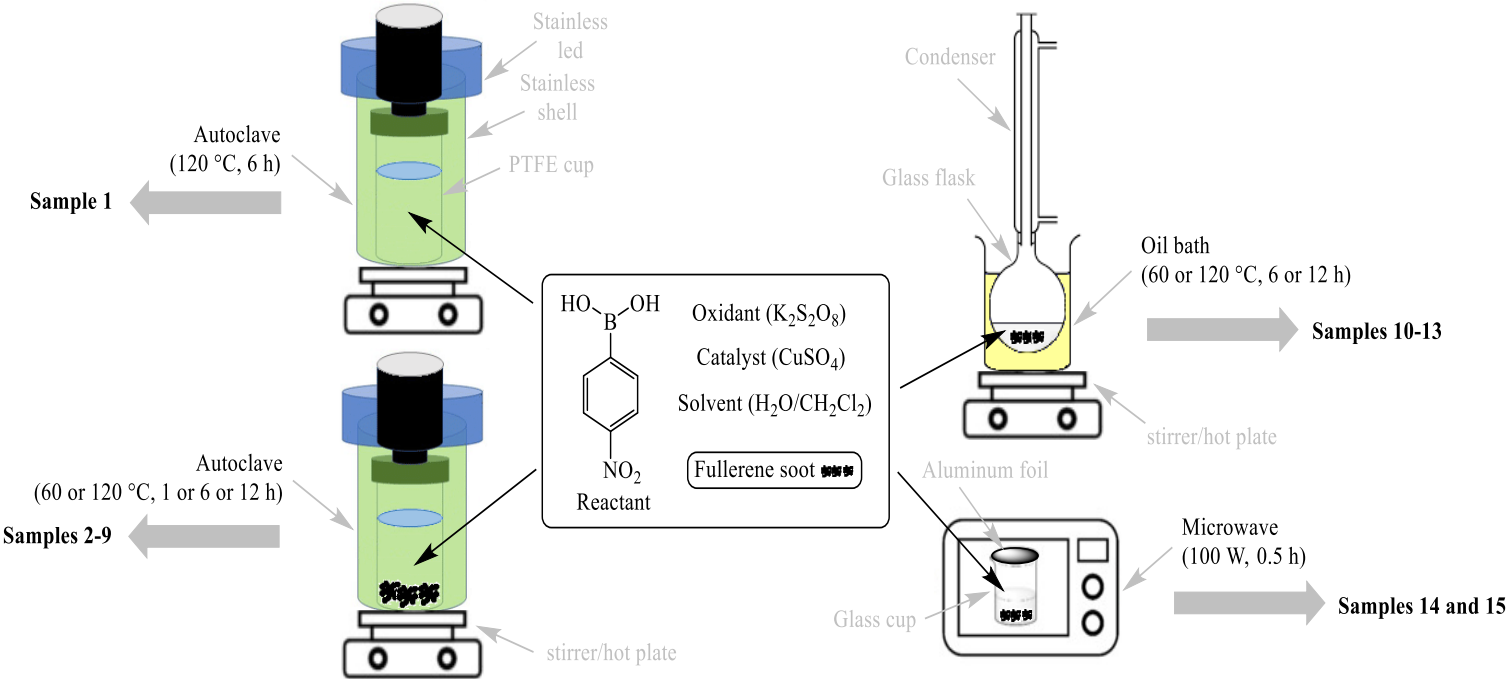

Figure 1. Experimental conditions used in this study (autoclave, oil-bath and microwave heating) for functionalizing fullerene soot nanoparticles with 4-nitrophenyl and 4-nitrophenoxy groups from the reaction of fullerene soot with 4-nitrophenylboronic acid (reactant) in the presence of potassium persulfate (oxidant) and copper(II) sulfate (catalyst) dissolved in water/dichloromethane (solvent)

There is an ionic equilibrium in the aqueous phase between the neutral and anionic forms of arylboronic acid [70]. The addition of H_2O to arylboronic acid is necessary to form the redox-active borate ($ArB(OH)_3^-$) [71], which is subsequently oxidized by persulfate or copper(II) or both when persulfate is present in large excess. In the absence of a catalyst (Fig. 2a), $ArB(OH)_3^-$ can transfer an electron to $SO_4^{\bullet-}$ to generate SO_4^{2-}. In the presence of a catalyst (Fig. 2b), $ArB(OH)_3^-$ can transfer an electron to Cu(II) to generate Cu(I). Then, Cu(I) reacts with $SO_4^{\bullet-}$ to generate Cu(II) and SO_4^{2-}. This process involves a catalytic cycle between Cu(I) and Cu(II) [72]. The aryl radical is formed as boric acid ($B(OH)_3$), leaving group eliminated [71]. Also, phenol (ArOH) can be derived from arylboronic acid in aqueous media (Fig. 2c) in the catalytic Cu or oxidant involved systems [62-64,73-76], even in the presence of fullerene [77]. The aryloxy ($ArO^{\bullet}$) radical is formed from the corresponding phenolic byproduct in the presence of persulfate/copper(II) (Fig. 2c). Catalysts such as Cu(II) salts have been used in the homolytic dissociation of alcohol/phenol O–H bonds [78]. It has been reported that 4-nitrophenoxy radical (4-$NO_2PhO^{\bullet}$) is the most favorable intermediate for the degradation of 4-nitrophenol (4-NO_2PhOH) in the aqueous phase [79]. However, 4-nitrophenoxy radical can undergo resonance to generate resonance-stabilized carbon-centered radicals [80]. The possible coupling products generated in thermally activated persulfate oxidation of nitrophenols are polynitrophenols, nitrated biphenyls, and nitrated diphenyl ethers, of which the latter two are formed by the combination of resonance-stabilized radicals [80].

Similarly, the diphenyl ether (Ar–O–Ar) and biphenyl (Ar–Ar) are identified as the coupling products of persulfate/silver(I) oxidation of arylboronic acid ($ArB(OH)_2$) in water/dichloromethane [53], confirming the formation of aryl and aryloxy radicals during the reaction. It is believed that the ether product originates from the radical species reacting with water to form phenol, which then undergoes a C–O coupling reaction to produce the ether product [53]. Since aryl and aryloxy radicals are less soluble in the aqueous phase [69], they can transfer to dichloromethane, where fullerene soot nanoparticles mainly exist.

The carbon-centered radicals add to the carbon-carbon π-bonds of fullerene soot, providing the new carbon-carbon σ-bonds [36]. The oxygen-centered radicals have a weak affinity to the addition mechanism [36]. The surface of soot is composed of many unpaired electrons (dangling bonds) with higher reactivity for scavenging both carbon- and oxygen-centered radicals [36,37,81,82]. The mechanistic explanation for the interactions of aryl and aryloxy radicals with the polyaromatic radicalic centers of fullerene soot through addition to C=C bonds and reacting with dangling bonds is illustrated in Figs. 2d and 2e, respectively.

3.2. Optimizing reaction for functionalizing fullerene soot

Experimental conditions used in this study for optimizing the reaction of fullerene soot with 4-nitrophenylboronic acid in the presence of potassium persulfate and copper(II) sulfate are presented in Table 1.

10.57647/ijc.2026.1601.06

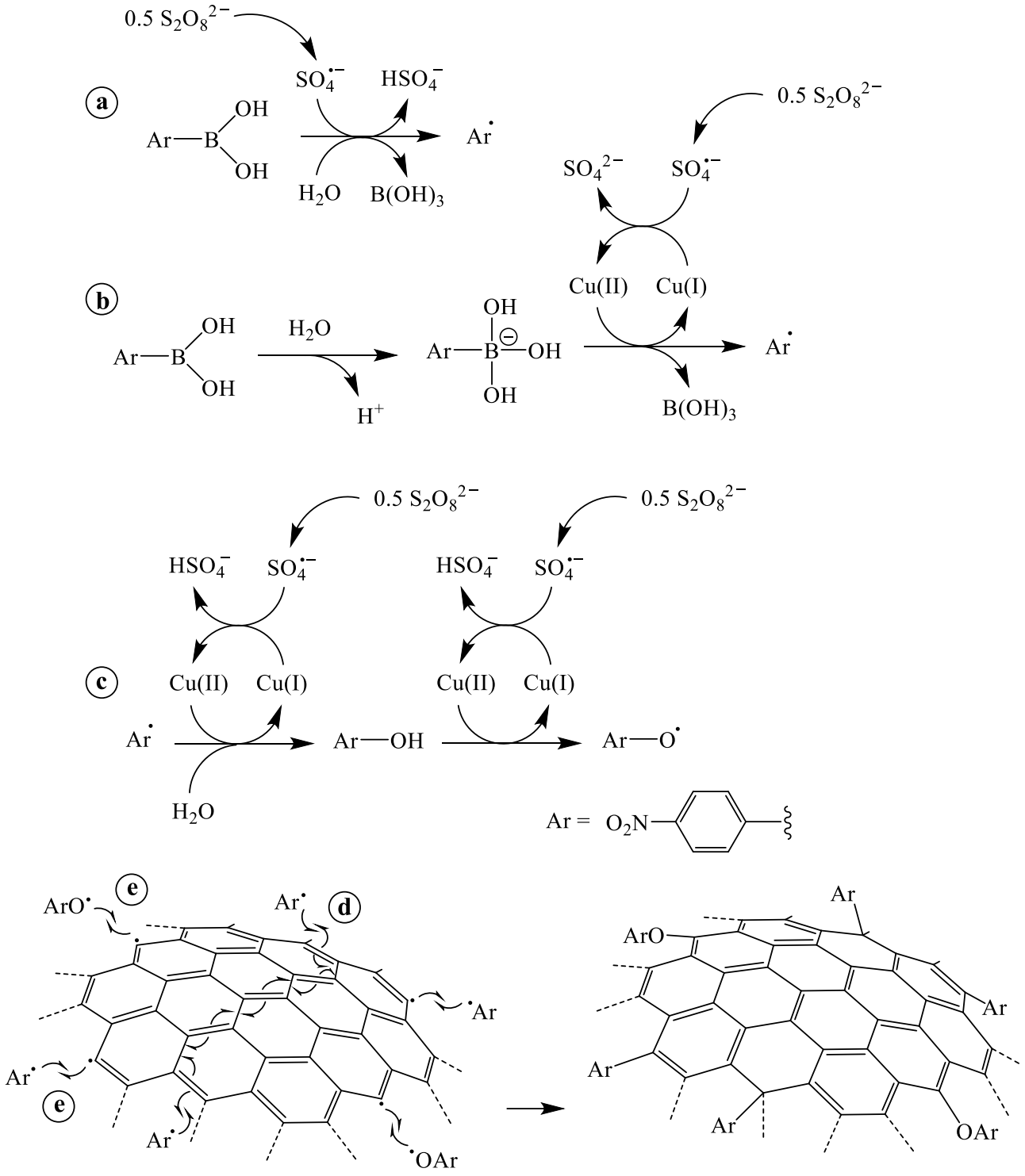

Figure 2. The proposed mechanisms for the formation of aryl (a, b) and aryloxy (c) radicals from arylboronic acid by employing persulfate ion as oxidant in the absence (a) or presence of copper(II) as catalyst (b, c), and the interactions of aryl and aryloxy radicals with the polyaromatic radicalic centers of fullerene soot through addition to C=C bonds (d) and reacting with dangling bonds (e)

To prepare samples with high nitrogen content, the reaction conditions for temperature (60 °C and 120 °C), time (0.5, 1, 6, and 12 hours), amounts of starting materials (equiv. or mmol ratios), and heating conditions (autoclave, oil-bath, and microwave) are optimized. The use of water/dichloromethane as bi-phasic solvent system is ideal for dissolving any polar and nonpolar byproducts. Dichloromethane has a low boiling point, so autoclave heating is recommended. Additionally, dichloromethane is a very low microwave absorbing solvent which can be heated to temperatures well above its boiling point [83]. The microwave heating is an eco-friendly and faster strategy than conventional heating methods to synthesize the nanomaterials and nanocomposites [84,85]. Sample 1 is a brown insoluble powder (Figure S1, supporting information) prepared in the absence of fullerene soot with equiv. ratio of 1:3:0.2 for reactant, oxidant, and catalyst in water/dichloromethane at 120 °C.

10.57647/ijc.2026.1601.06

Table 1. Optimizing reaction conditions for functionalizing fullerene soot nanoparticles with 4-nitrophenyl and 4-nitrophenoxy groups using copper-catalyzed oxidative deboration of 4-nitrophenylboronic acid (reactant) in the presence of potassium persulfate (oxidant) and copper(II) sulfate (catalyst) dissolved in water/dichloromethane (solvent)

Sample number	Fullerene soot (mg)	Reactant Equiv. (mmol)	Oxidant Equiv. (mmol)	Catalyst Equiv. (mmol)	Heating type	Temperature (°C)	Time (h)
1	-	1 (0.125)	3 (0.375)	0.2 (0.025)	Autoclave	120	6
2	15	1 (0.125)	3 (0.375)	0.2 (0.025)	Autoclave	120	6
3	15	1 (0.125)	3 (0.375)	0.2 (0.025)	Autoclave	120	12
4	15	1 (0.125)	3 (0.375)	0.2 (0.025)	Autoclave	120	1
5	15	1 (0.125)	3 (0.375)	0.2 (0.025)	Autoclave	60	6
6	15	-	3 (0.375)	0.2 (0.025)	Autoclave	120	6
7	15	1 (0.125)	1 (0.125)	0.2 (0.025)	Autoclave	120	6
8	15	1 (0.125)	3 (0.375)	-	Autoclave	120	6
9	15	1 (0.125)	3 (0.375)	1 (0.125)	Autoclave	120	6
10	15	1 (0.125)	3 (0.375)	-	Oil-bath	60	12
11	15	1 (0.125)	3 (0.375)	0.2 (0.025)	Oil-bath	60	12
12	15	1 (0.125)	3 (0.375)	0.2 (0.025)	Oil-bath	120	12
13	15	1 (0.125)	3 (0.375)	0.2 (0.025)	Oil-bath	120	6
14	15	1 (0.125)	3 (0.375)	-	Microwave	100 W	0.5
15	15	1 (0.125)	3 (0.375)	0.2 (0.025)	Microwave	100 W	0.5

According to the literature review [53,80,86-98] and further analysis described in the next sections, sample 1 might be an amorphous solid containing 4-nitrophenoxy groups involved in ether linkages produced from the coupling of the corresponding aryloxy radicals. The C–O coupling of aryloxy radicals produces the ether linkages, while the C–C coupling of aryloxy radicals leads to the formation of quinone moieties [86]. When the reaction is carried out under the same conditions but without water, this product cannot be formed, because it is formed from the corresponding phenolic byproduct in water.

Samples 2-15 are the black insoluble powders prepared in the presence of fullerene soot and various equiv. ratios of reactant, oxidant and catalyst in water/dichloromethane at 60 and 120 °C or 100 W. Sample 6 is prepared in the absence of reactant with equiv. ratio of 3:0.2 for oxidant and catalyst. In this condition, the oxidation of C=C bonds of fullerene soot can occur. Samples 8, 10 and 14 are prepared in the absence of catalyst with equiv. ratios of 1:3 for reactant and oxidant in different heating conditions. The other samples are prepared with equiv. ratios of 1:3:0.2, 1:3:1 and 1:1:0.2 for reactant, oxidant and catalyst. In both absence or presence of catalyst, aryl (i.e. 4-nitrophenyl) and aryloxy (i.e. 4-nitrophenoxy) radicals are efficiently trapped by fullerene soot nanoparticles to eventually afford samples with high nitrogen contents. The potential applications of the high nitrogen content samples could include high-energy materials such as explosives, propellants, or other advanced energetic materials [99]. Also, the nitrogen-containing carbon materials could be designed for use in energy conversion and storage, catalysis, sensors, electronic nanodevices, environmental protection, and biology-related applications [100-102].

3.3. Characterization of fullerene soot after functionalizing

3.3.1. *EDX line scan and elemental maps*

SEM-EDX elemental maps of the main samples 2 (prepared in the presence of reactant, oxidant, and catalyst), 6 (prepared in the presence of oxidant and catalyst), and 8 (prepared in the presence of reactant and oxidant) are shown in Figs. 3-5, respectively. The corresponding data for the other samples are indicated in the supporting information (Figures S2-S6). The prepared sample in the absence of reactant (4-NO_2PhB$(OH)_2$) has only C, O, S, K, and Cu elements identified by EDX spectrum (Fig. 4). The prepared sample in the absence of a catalyst ($CuSO_4$) contains C, O, N, S, and K elements (Fig. 5). The prepared sample in the presence of reactant and catalyst has all the C, O, N, S, K, and Cu elements (Fig. 3).

Since fullerene soot does not contain nitrogen (EDX analysis of this compound shows only the presence of C and O elements [17]), the presence of N in the prepared samples is attributed to the successful functionalization of fullerene soot nanoparticles with 4-nitrophenyl and 4-nitrophenoxy groups. The averages of elemental composition calculated from EDX line scan (15 data points) for the selected samples are listed in Table 2. According to these data and elemental maps shown in Fig. S1, sample 1, prepared in the absence of fullerene soot, contains 70.03 wt.% C, 17.53 wt.% O and 10.33 wt.% N along with relatively small amounts of S, K, and Cu impurities (2.10 wt.%) trapped in the sample texture. The oxygen content in this sample is greater than the nitrogen, suggesting this sample contains higher ether linkages.

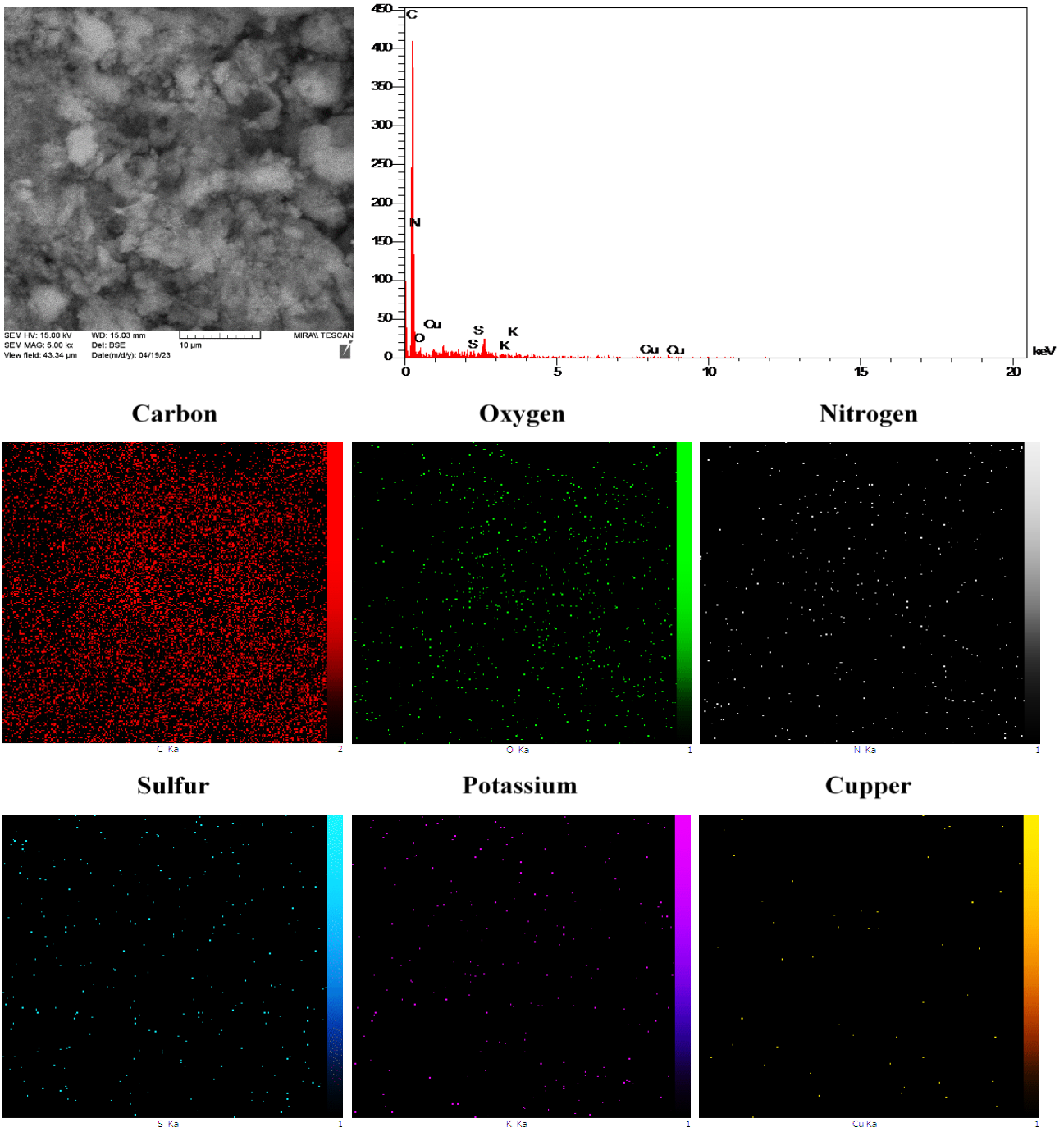

Figure 3. SEM-EDX elemental maps of sample 2 (prepared with 1 equiv. of 4-NO_2PhB$(OH)_2$ as reactant, 3 equiv. of $K_2S_2O_8$ as oxidant and 0.2 equiv. of $CuSO_4$ as catalyst in autoclave at 120 °C for 6 h)

The EDX line scan and elemental maps of sample 6 (Fig. 4), prepared in the absence of reactant, show only the presence of C (89.67 wt.%) and O (8.35 wt.%) elements along with the small amounts of S, K, and Cu (1.98 wt.%). While the EDX line scan and elemental maps of sample 2 (Fig. 3), prepared under similar conditions in the presence of reactant, show a significant amount of N (17.24 wt.%) along with C (72.00 wt.%), O (9.52 wt.%), and small amounts of S, K, and Cu elements (1.23 wt.%).The nitrogen content in this sample is greater than oxygen, indicating a higher number of 4-nitrophenyl than 4-nitrophenoxy groups. All of the other samples prepared in the presence of reactant also have significant nitrogen contents (6.69 to 19.60 wt.%), which are higher than the previously reported values for the samples prepared by other radical precursors (i.e. nitroaryl diazoniums (6.27 wt.% [17]), nitroaryl carboxylic acids (6.10 wt.% [21]) and nitroaryl carboxylates (5.79 wt.% [27]). These results confirm the successful functionalization of fullerene soot nanoparticles using copper-catalyzed oxidative deboration of 4-nitrophenylboronic acid. The EDX line scan and elemental maps of sample 4 (Figure S2), prepared with a shorter reaction time (1 h) than sample 2 (6 h) at the same temperature (120 °C) and other conditions, do not indicate a significant variation in the nitrogen content (17.48 wt.%).

10.57647/ijc.2026.1601.06

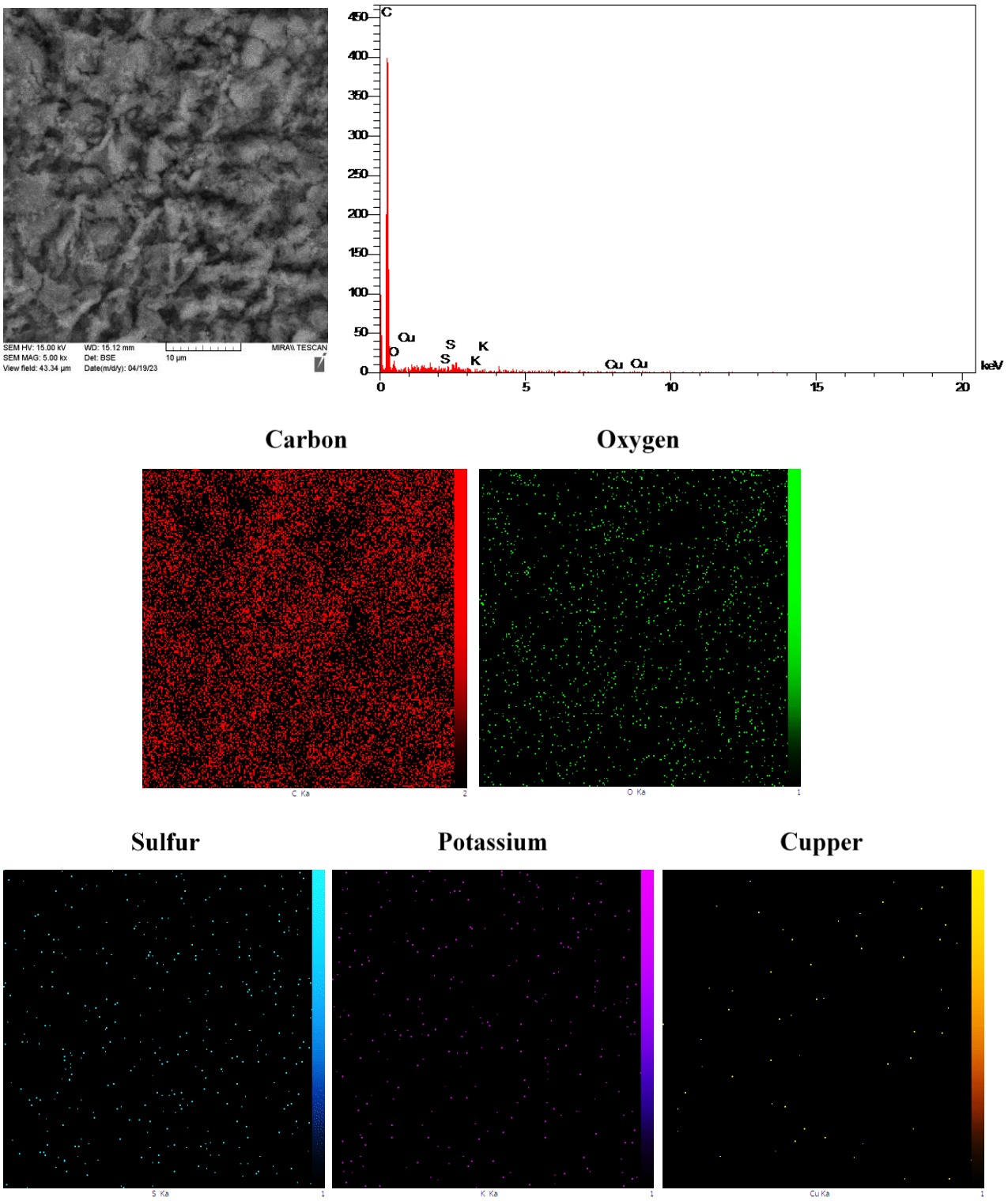

Figure 4. SEM-EDX elemental maps of sample 6 (prepared with 3 equiv. of $K_2S_2O_8$ as oxidant and 0.2 equiv. of $CuSO_4$ as catalyst in autoclave at 120 °C for 6 h, in the absence of 4-NO_2PhB$(OH)_2$ as reactant)

Although the oxygen content in this sample decreases (6.59 wt.%). These results show that functionalizing fullerene soot can occur in shorter reaction times. However, in the longer reaction times, the surface of fullerene soot is more oxidized, which leads to increased oxygen content. The EDX line scan and elemental maps of sample 5 (Figure S3), prepared at the lower reaction temperature (60 °C), compared to sample 2 (120 °C), with the same reaction time (6 h) and other conditions, do not indicate a significant variation in the nitrogen content (17.17 wt.%). Although the oxygen content in this sample decreases (6.97 wt.%). These results confirm successfully functionalizing fullerene soot by 4-nitrophenylboronic acid at the lower reaction temperatures. However, at the higher temperatures, more oxidation of the fullerene soot occurs, which results in an increase in the oxygen content. The oxidant to reactant equiv. ratio of 3:1 is used in the preparation of the samples described above.

10.57647/ijc.2026.1601.06

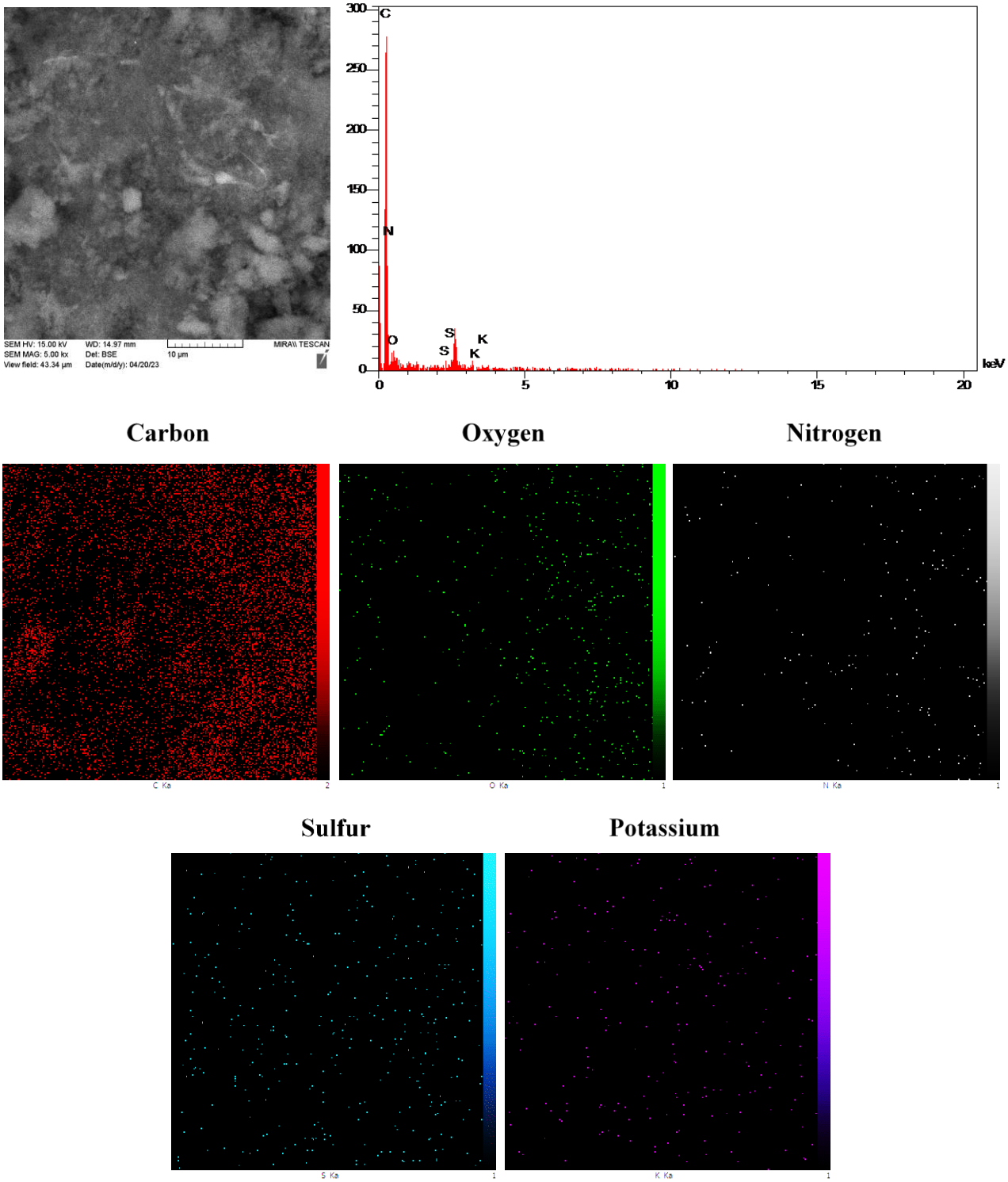

Figure 5. SEM-EDX elemental maps of sample 8 (prepared with 1 equiv. of 4-NO_2PhB$(OH)_2$ as reactant and 3 equiv. of $K_2S_2O_8$ as oxidant in autoclave at 120 °C for 6 h, in the absence of $CuSO_4$ as catalyst)

To check the influence of the oxidant, the preparation of sample 7 is carried out on the oxidant to reactant equiv. ratio of 1:1, while the other conditions are constant. The EDX line scan and elemental maps of sample 7 (Figure S4) do not show a significant variation in oxygen (9.36 wt.%) and nitrogen (16.82 wt.%) contents compared to sample 2, indicating that the reaction occurs successfully with an equiv. amount of oxidant. The catalyst to reactant equiv. ratio of 0.2:1 is used in the preparation of the samples described above.

To check the influence of the catalyst, functionalizing fullerene soot is performed in the absence of the catalyst. The EDX line scan and elemental maps of sample 8 (Figure 5) show the lower nitrogen (16.29 wt.%) and oxygen (7.23 wt.%) contents compared to sample 2. The presence of the significant content of nitrogen in this sample confirms that the reaction of fullerene soot with 4-nitrophenylboronic acid occurs even in the absence of catalyst. However, 0.2 equiv. copper(II) catalyst can be used to obtain samples with more nitrogen content.

10.57647/ijc.2026.1601.06

Table 2. The average of elemental composition calculated by EDX line scan (15 data points) of the selected samples

Sample number	Weight% (Atomic%)					
	C	O	N	S	K	Cu
1	70.03 (75.66)	17.53 (14.26)	10.33 (9.60)	0.17 (0.07)	0.17 (0.06)	1.76 (0.36)
2	72.00 (76.42)	9.52 (7.59)	17.24 (15.71)	0.10 (0.04)	0.10 (0.03)	1.03 (0.21)
4	73.97 (78.39)	6.59 (5.25)	17.48 (15.91)	0.19 (0.08)	0.16 (0.05)	1.61 (0.32)
5	73.85 (78.34)	6.97 (5.55)	17.17 (15.65)	0.18 (0.07)	0.16 (0.05)	1.67 (0.34)
6	89.67 (93.06)	8.35 (6.51)	-	0.14 (0.06)	0.15 (0.05)	1.69 (0.33)
7	72.22 (76.77)	9.36 (7.51)	16.82 (15.33)	0.19 (0.08)	0.26 (0.09)	1.15 (0.23)
8	75.85 (79.43)	7.23 (5.69)	16.29 (14.66)	0.32 (0.13)	0.31 (0.10)	-
9	73.33 (77.86)	10.34 (8.25)	14.87 (13.56)	0.11 (0.05)	0.13 (0.04)	1.22 (0.24)
10	34.50 (40.81)	56.99 (51.64)	6.69 (6.83)	0.69 (0.31)	1.14 (0.42)	-
11	65.34 (70.10)	13.94 (11.62)	19.60 (18.01)	0.11 (0.04)	0.10 (0.03)	0.91 (0.19)

In the following, the catalyst to reactant equiv. ratio of 1:1 is used for the preparation of sample 9. The EDX line scan and elemental maps of sample 9 (Figure S5) indicate a significant decrease in nitrogen (14.87 wt.%) and a significant increase in oxygen (10.34 wt.%), when the amount of catalyst is increased. Therefore, in the presence of extra amounts of catalyst and/or oxidant, the surface of fullerene soot is more oxidized. Additionally, using 1 equiv. copper(II) catalyst leads to decrease in nitrogen content.

All samples described above are prepared under autoclave heating conditions. To investigate the influence of the type of heating, samples 10 and 11 are prepared in the absence and presence of a catalyst in an oil-bath heating at 60 °C, respectively. The EDX line scan and elemental maps (Figure S6) show the more significant changes compared to the samples prepared in an autoclave, so that in the presence of the catalyst, the nitrogen content is increased from 6.69 to 19.60 wt.% and the oxygen content is decreased from 56.99 to 13.94 wt.%. According to the results of Table 2 and elemental maps, sample 11 was prepared in the presence of a catalyst with equiv. ratio of 1:3:0.2 for reactant, oxidant and catalyst in an oil-bath heating conditions has higher nitrogen content among other samples.

3.3.2. *FT-IR spectral analysis*

FT-IR spectra of the selected samples prepared in different conditions compared to fullerene soot are shown in Figure 6. FT-IR spectrum of the sample 1 containing 4-nitrophenoxy groups (Figure 6a) indicates the significant peaks at 3433 cm^{-1} (OH stretching), 1488 and 1612 cm^{-1} (C=C stretching), 1643 cm^{-1} (C=O stretching of quinone), 1060 and 1122 cm^{-1} (C–O stretching), and 1350 and 1581 cm^{-1} (NO_2 stretching).

The presence of a sharp characteristic peak at 1207 cm^{-1} in this sample is attributed to the Ph–O–Ph linkages. These assignments are supported by previous findings about a series of polymeric compounds with similar functional groups. For instance, the strong peak appeared at about 1245 cm^{-1} in the FT-IR spectrum of 2,2'-bis(p-phenoxyphenyl)-4,4'-dinitrodiphenyl ether demonstrates the presence of Ph–O–Ph linkages [94]. Also, the strong peaks appeared at 1345 and 1588 cm^{-1} of this compound are due to symmetric and asymmetric stretching of NO_2 groups, respectively [94]. The Ph–O–Ph linkages in the FT-IR spectrum of 1,1-bis [4-(4-nitro-2-trifluoromethylphenoxy) phenyl]-1-phenyl-2,2,2-trifluoroethane appear at 1268 cm^{-1} [95].

The nitro groups of this compound give two characteristic bands at 1353 and 1533 cm^{-1} [95]. A strong band seen at 1610 cm^{-1} in the FT-IR spectrum of poly(phenylene oxide) is indicative of C=O stretching [96]. The peaks at 1467 and 1601 cm^{-1} of this compound are corresponded to the C=C vibrations and the peak at 1180 cm^{-1} is referred to the vibration of C–O bond [89]. The peak at 1196 cm^{-1} in the FT-IR spectrum of poly(phenylene oxide) is assigned to the C–O stretching vibrations of phenylene oxide [97]. The peak at the 1207 cm^{-1} region represents the ether groups (Ph–O–Ph) of poly(phenylene oxide) [98].

FT-IR spectrum of fullerene soot (Figure 6g) is relatively simple [21,27] and indicates weak peaks belonging to OH (3444 cm^{-1}), C=C (1458 and 1620 cm^{-1}), C=O (1735 cm^{-1}), and C–O (1084 cm^{-1}) groups. The intensity of these peaks increases significantly, and the characteristic absorption bands of the nitro group appear in the samples functionalized by 4-nitrophenylboronic acid.

The main peaks in the FT-IR spectra of functionalized fullerene soot samples 2 (Figure 6b), 8 (Figure 6d), 10 (Figure 6e), 13 (Figure 6c) and 15 (Figure 6f) belong to OH stretching (3429 to 3470 cm^{-1}), C=C stretching (1423 to 1485 and 1627 to 1651 cm^{-1}), C=O stretching (1700 to 1766 cm^{-1}), C–O stretching (1049 to 1223 cm^{-1}), NO_2 symmetric stretching (1358 to 1361 cm^{-1}) and NO_2 asymmetric stretching (1531 to 1593 cm^{-1}) vibrations. The stretching vibration peak of Ph–O–Ph linkages is seen at near 1207 cm^{-1}. These results confirm the successful functionalization of fullerene soot with both 4-nitrophenyl and 4-nitrophenoxy groups.

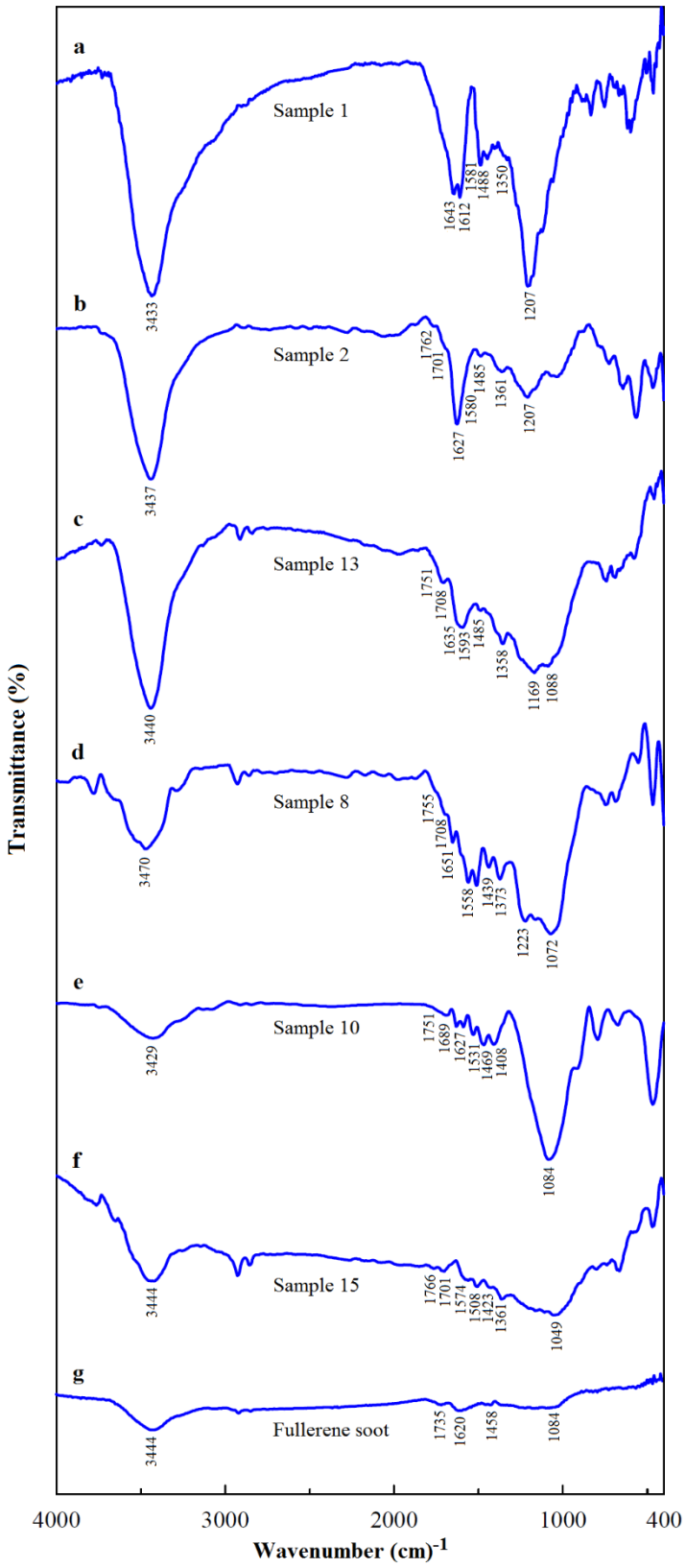

Figure 6. FT-IR spectra of the selected samples 1 (a), 2 (b), 8 (d), 10 (e), 13 (c) and 15 (f) compared to fullerene soot (g)

3.3.3. *XRD measurements*

XRD patterns for the selected samples prepared in different heating conditions in the absence or presence of catalyst, compared to fullerene soot, are shown in Figure 7.

The XRD pattern of fullerene soot shows a broad region of diffracted intensity between 2θ angles of 10 to 50 with maximum intensity at 2θ = 25° [17], which is very closein position to the (002) reflection in graphite [103]. However, the XRD peak is broad, which is indicative of the amorphous nature of this compound.

10.57647/ijc.2026.1601.06

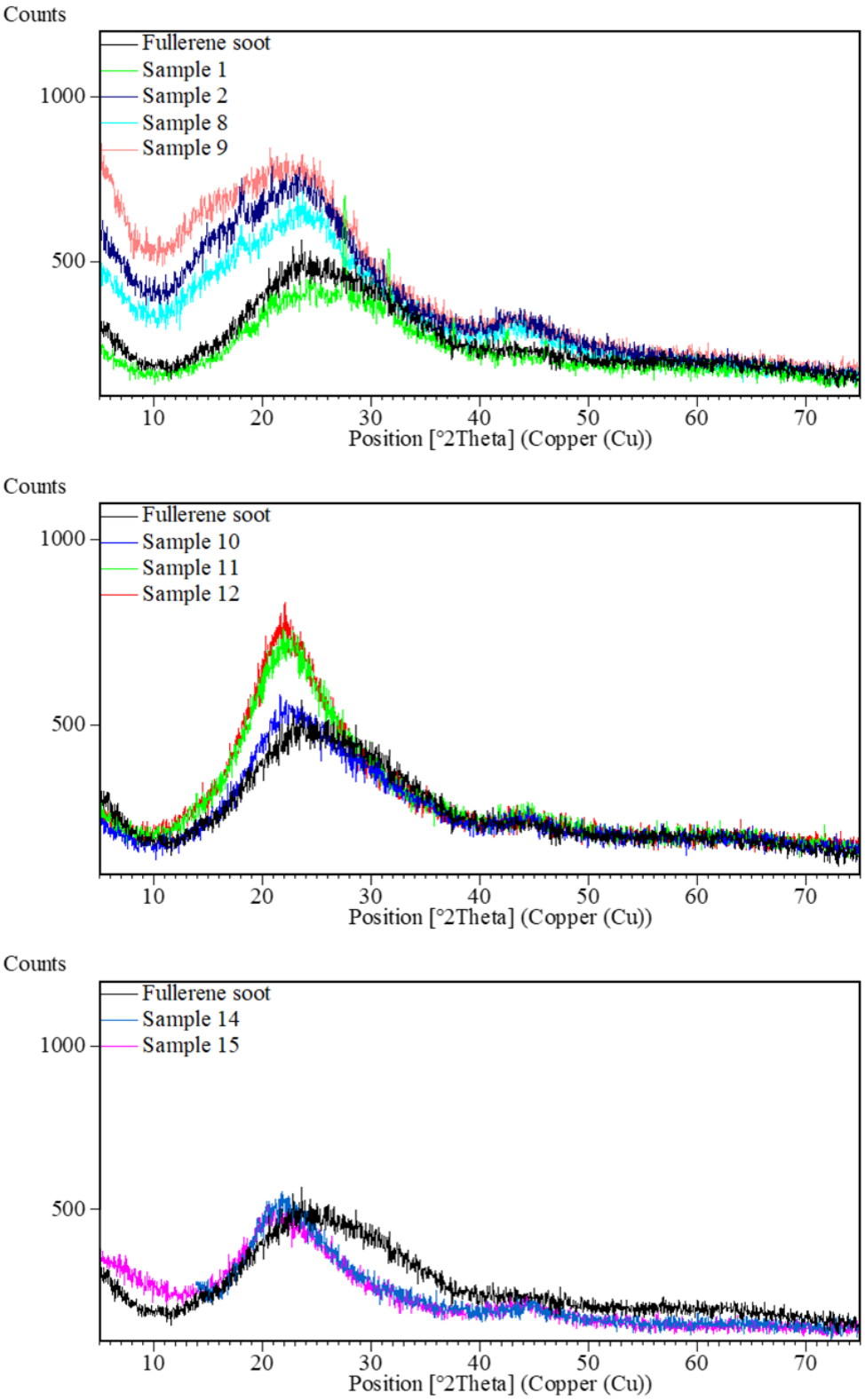

Figure 7. XRD patterns of the selected samples prepared in autoclave (samples 1, 2, 8 and 9), oil-bath (samples 10-13) and microwave (samples 14 and 15) compared to fullerene soot

The sample 1 consists of both crystalline and amorphous regions. The sharp diffraction peaks of this sample at 2θ = 27.6, 31.6, 37.6, 42.5, and 46.0° may be due to impurity. These peaks are matched with the main peaks of $K_2S_2O_8$ (JCPDS 00-012-0483), K_2SO_4 (JCPDS 01-081-0190), CuO (JCPDS 01-078-0428), and Cu_2O (JCPDS 01-075-1531). The diffraction pattern of the amorphous region shows a continuous background at 2θ = 10-40°, like those known for amorphous polymers such as poly(2,6-dimethyl-1,4-phenylene)oxide (2θ = 5-30°) [104,105] and polyamides derived from 2,2'-bis(p-phenoxyphenyl)-4,4'-diaminodiphenyl ether (2θ = 10-40°) [94]. The XRD patterns of the selected functionalized fullerene samples 2-15 are also amorphous.

10.57647/ijc.2026.1601.06

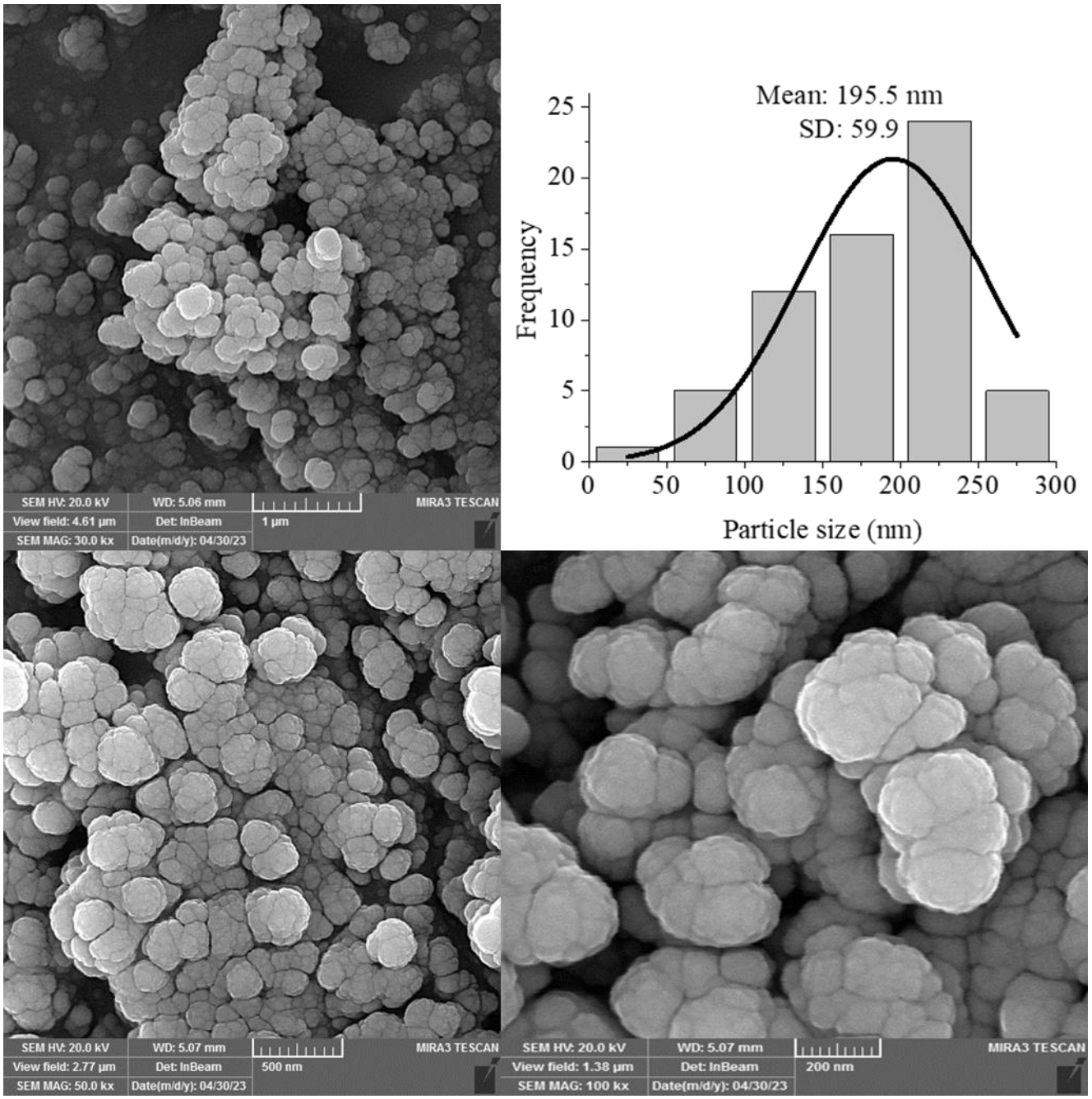

Figure 8. FESEM images and particle size histogram of sample 2 (prepared in autoclave)

However, the significant difference in the intensity, width, and position of the diffraction patterns of the samples prepared under different heating conditions in the presence or absence of the catalyst, compared to the fullerene soot, can be seen. These changes are much more pronounced for the samples prepared in the presence of the catalyst. The XRD patterns for samples 2, 8, and 9 prepared under an autoclave (Figure 7, top) are wider, while samples 14 and 15 prepared under a microwave (Figure 7, bottom) are narrower. Also, the XRD patterns of the samples 11 and 12 prepared under oil-bath heating seem sharper (Figure 7, middle). Therefore, the samples prepared in an autoclave have a more amorphous nature than the samples prepared in an oil bath and a microwave, because heat and pressure during the reaction in an autoclave cause a rise in the amorphism degree of the product. The samples obtained with microwave due to low microwave power in a short reaction time have less amorphous character. The oil-bath heating with a higher functionalization degree is found to enhance the crystallinity of the product.

3.3.4. *FESEM analysis*

FESEM images and particle size distribution histogram for samples 2, 13, and 15 prepared with the same equiv. ratio of starting materials but under different heating conditions (autoclave, oil-bath, or microwave) are shown in Figures 8-10, respectively. These data for pure fullerene soot can be seen in our previous publications [17,21,27].

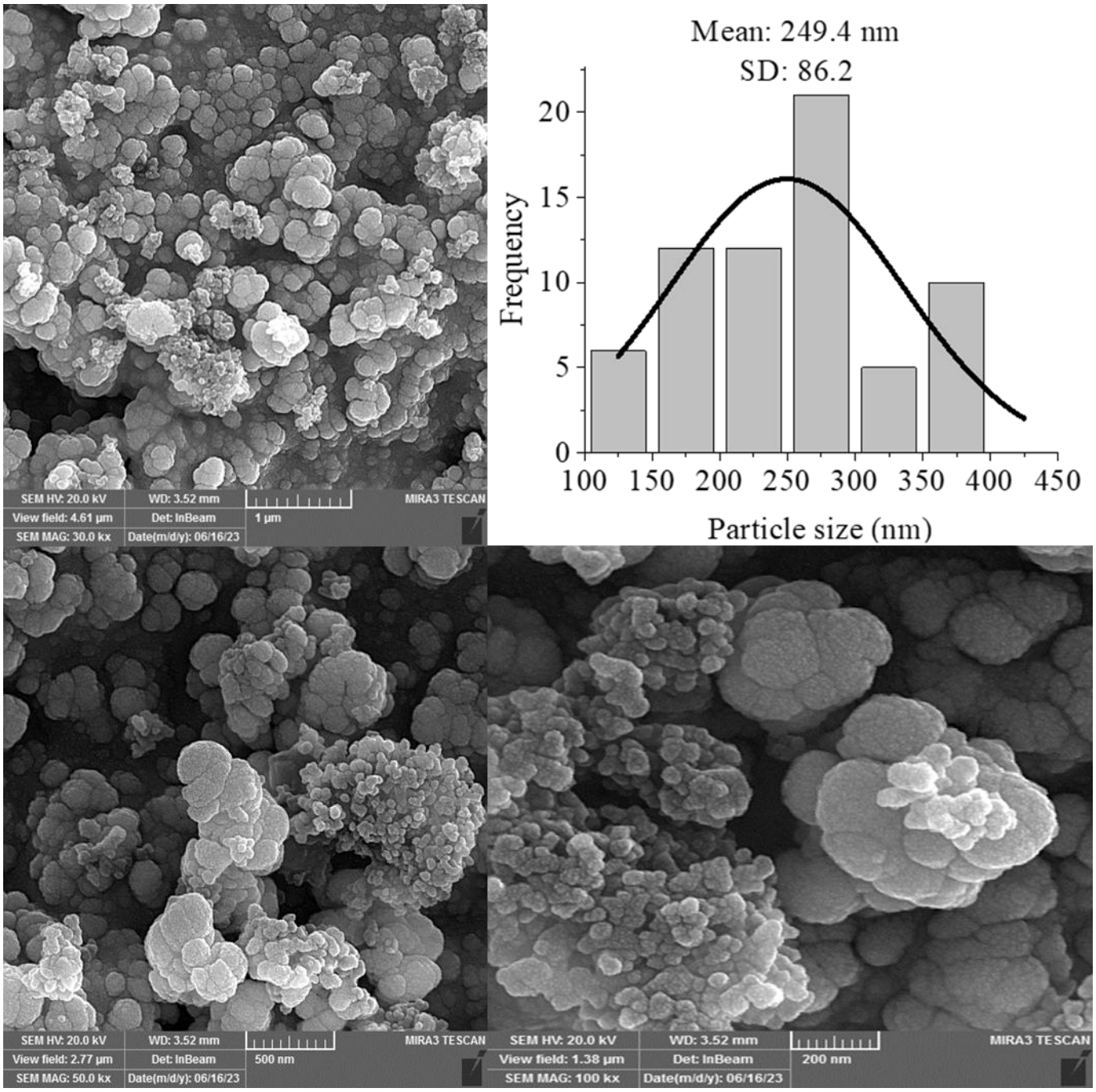

Figure 9. FESEM images and particle size histogram of sample 13 (prepared in oil-bath)

Fullerene soot has a narrower range of particle sizes (20-100 nm) with the average particle size of 48.9 nm [17,21,27]. While the fullerene soot samples functionalized with 4-nitrophenyl and 4-nitrophenoxy groups have greater average particle sizes and broadened particle size distributions (20 to 450 nm). The average particle size in sample 2 prepared under an autoclave, is 195.5 nm, which is smaller than that for samples 13 (249.4 nm) and 15 (245.6 nm) prepared under an oil bath and microwave, respectively. According to FESEM images, the morphology of fullerene soot after functionalizing is spherical; however, the samples prepared under autoclave and microwave have a more uniform texture than the sample prepared in an oil bath. Microwave gives homogenous heating to the reaction mixture, which leads to the formation of samples with a uniform size. The aging time in the autoclave promotes the formation of uniform-sized nanoparticles.

3.3.5. *TGA-DSC analysis*

TGA-DSC thermograms in an air atmosphere for the selected samples are shown in Figure 11. The results of this analysis for fullerene soot can be seen in our previous publication [21]. The total weight loss from room temperature to 850 °C for fullerene soot is 98.3 % [21], which suggests that the decomposition of this compound is nearly complete.

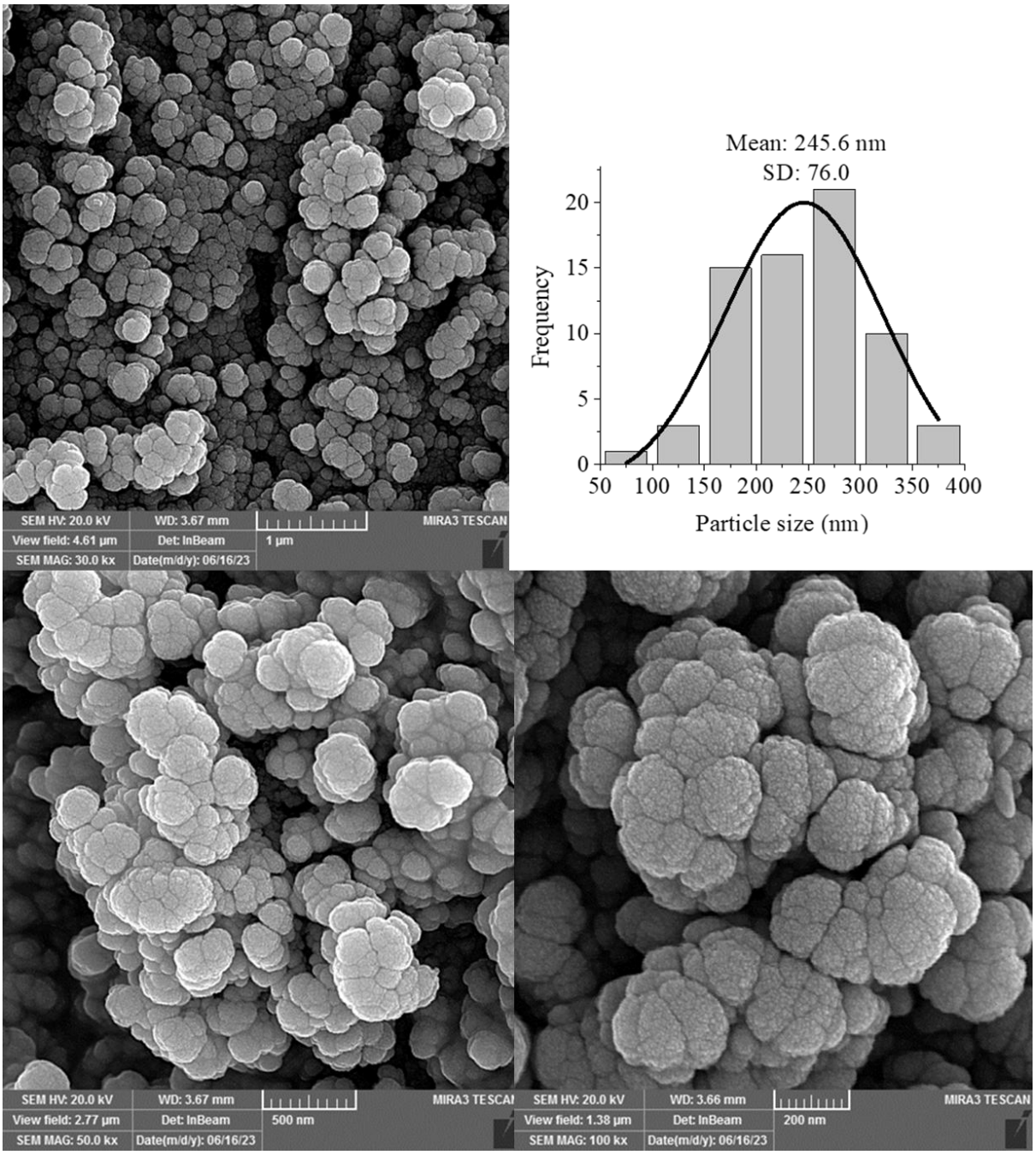

Figure 10. FESEM images and particle size histogram of sample 15 (prepared in microwave)

The amorphous solid sample 1 and the selected functionalized fullerene soot samples, during heating until 850 °C, undergo decomposition with 13-32 % remaining residue. The final residue is probably due to the mixture of inorganic and carbonaceous matter. The presence of inorganic matter in the texture improves the thermal stability of the prepared samples compared to fullerene soot. Fullerene soot is thermally stable up to 360 °C [21]. The weight loss of fullerene soot below this temperature is 1.9 % [21]. The weight loss during the decomposition of fullerene soot at 360-690 °C is 95.9 % [21].

The weight loss of fullerene soot above this range is 0.5 % [21]. Thermal decomposition of sample 6 (Fig. 11a) prepared in the absence of 4-nitrophenylboronic acid proceeds through the sample weight loss below 150 °C (5.6 %), 150-360 °C (13.7 %), 360-600 °C (25.1 %), and above 600 °C (24.0 %). The surface of nanoparticles in this sample is functionalized by –OH and –COOH groups generated during the oxidation of fullerene soot by persulfate/copper(II).

The weight loss below 150 °C is generally corresponds to the loss of adsorbed water [106]. The loss of organic functional groups occurs below 360 °C [107,108], while decomposition of fullerene soot [21] needs higher temperatures.

Like fullerene soot, there is no exothermic peak observed in the DSC thermogram of sample 6. For the samples prepared in the presence of 4-nitrophenylboronic acid, an exothermic peak attributed to the decomposition of energetic groups is observed.

10.57647/ijc.2026.1601.06

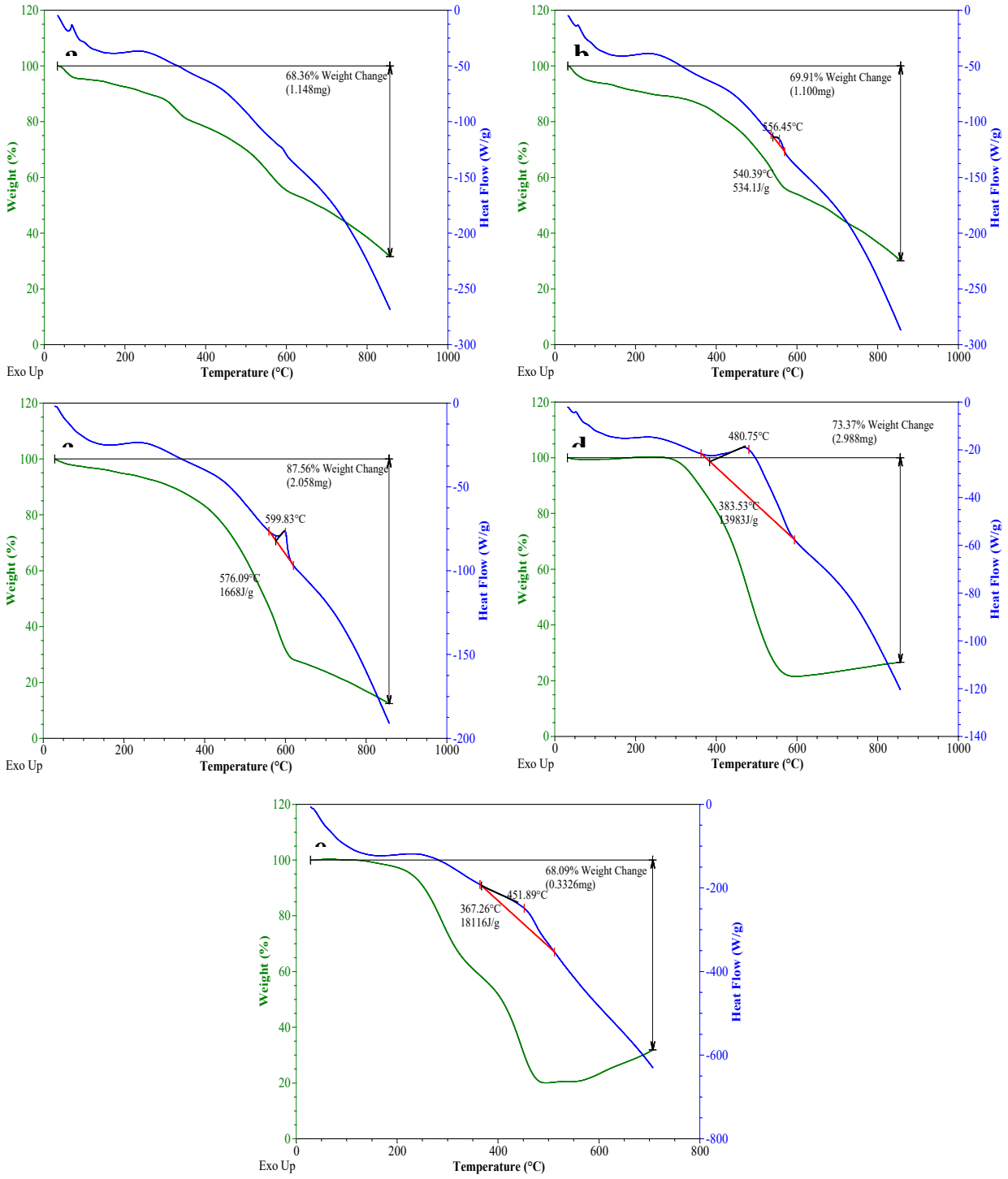

Figure 11. TGA-DSC thermograms of the selected samples 1 (e), 2 (b), 3 (c), 6 (a) and 12 (d) in air atmosphere

The surface of nanoparticles in these samples is functionalized by –OH, –COOH, 4-NO_2Ph–, and 4-NO_2PhO– groups. Decomposition of 4-nitrophenyl and 4-nitrophenoxy groups is exothermic, which occurs at 360-600 °C. DSC thermogram of sample 2 (Fig. 11b) prepared with equiv. ratio of 1:3:0.2 for reactant, oxidant and catalyst at 120 °C for 6 h under autoclave shows a relatively small exothermic peak with a heat release of 534.1 J/g around 556 °C. The most significant weight loss in the TGA thermogram of this sample occurs between 250 and 600 °C (35.7 %). The weight loss below and above this range is 10.3 and 23.9 %, respectively. DSC thermogram of sample 3 (Fig. 11c) prepared under similar conditions but with the longer reaction time (12 h) indicates a stronger exothermic peak started at 576 °C with a heat release of 1668 J/g. The most significant weight loss in the TGA thermogram of this sample occurs between 200 and 650 °C (68.1 %). The weight loss below and above this range is 5.2% and 14.3 %, respectively. The total weight loss for sample 3 is higher than that for sample 2 (87.6 % versus 69.9 %), which indicates that this sample is more functionalized with energetic groups in the

10.57647/ijc.2026.1601.06

longer reaction times. The best energetic performance is obtained for sample 12, prepared in the same conditions, but under oil-bath heating. DSC thermogram of this sample (Fig. 11d) shows a higher broad exotherm started at 383 °C with a heat release of 13983 J/g and peak maximum temperature of 480 °C. The most significant weight loss in the TGA thermogram of this sample occurs between 350 and 600 °C (78.4 %). These results agree with previous investigations.

For instance, the nitro aromatic compounds show mild exothermic activity at 300-350 °C, after which there are relatively large exotherms around 450 °C [109]. The single-walled carbon nanotubes functionalized with NO_2Ar– groups show exothermic peaks at 300-330 °C [19]. The fullerene soot functionalized with NO_2Ar– groups show exothermic decomposition at 400-600 °C [21].

The pure 4-nitrophenol exothermically decomposes at 260 °C [110]. Compared to nitrophenols, the exothermic peaks of nitrophenolates are more intense [111]. It has been reported that the violent decomposition of nitrophenols is caused by the intermolecular catalysis effect of the nitrophenoxy groups [111]. In consistent with these data, the amorphous solid sample 1 contained 4-nitrophenoxy groups, which also have energetic potential. DSC thermogram of this sample (Fig. 11e) indicated a strong exothermic peak started at 367 °C with a heat release of 18116 J/g and peak maximum temperature of 452 °C.

The most significant weight loss in the TGA thermogram of this sample occurs below 360 °C (40.7 %) and 360-500 °C (39.2 %). The increase in weight at temperatures higher than 500 °C is generally attributed to the further oxidation of residual inorganic matter [26]. This sample is like the nitro-substituted cyclic oligomers of phenol (decomposition temperatures 363-376 °C), which can be considered as a nitro-based thermally stable energetic compound with ether linkages [112,113].

4. Conclusions

In this study, 4-nitrophenylboronic acid was used as a radical precursor for functionalizing fullerene soot nanoparticles with 4-nitrophenyl and 4-nitrophenoxy groups. The formation mechanisms of 4-nitrophenyl and 4-nitrophenoxy radicals from oxidative deboration of 4-nitrophenylboronic acid by employing potassium persulfate as oxidant and copper (II) sulfate as catalyst were discussed.

To obtain samples with high nitrogen contents, the reaction conditions were optimized against temperature, time, and the amounts of starting materials. The characterization of products was performed by EDX and elemental mapping, FT-IR, XRD, FESEM, and TGA-DSC.

Since fullerene soot and the sample prepared in the absence of 4-nitrophenylboronic acid do not contain nitrogen, the presence of nitrogen in the EDX data of the samples prepared in the presence of 4-nitrophenylboronic acid is attributed to the successful functionalization of fullerene soot.

The prepared samples have up to 19.60 wt.% nitrogen, which is higher than the previously reported values for the samples prepared by other radical precursors (i.e., nitroaryl diazoniums, nitroaryl carboxylic acids, and nitroaryl carboxylates). The reaction could occur even in the absence of a catalyst. However, a catalyst could be used to obtain samples with more nitrogen content and better energetic performance.

The equiv. ratio of 1:3:0.2 for reactant, oxidant and catalyst is preferred than 1:3:0, 1:3:1 and 1:1:0.2. The nitrogen content in samples prepared in autoclave is greater than the oxygen, indicating the higher number of 4-nitrophenyl groups than 4-nitrophenoxy groups. At higher temperatures or in longer reaction times or in the presence of extra amounts of catalyst and oxidant, the surface of fullerene soot is more oxidized.

The highest oxygen content is found for the sample prepared with excess oxidant and without catalyst in oil-bath. The characteristic absorption bands of $–NO_2$ and Ph–O–Ph groups are observed in FT-IR spectra of the samples functionalized by 4-nitrophenylboronic acid. The XRD patterns of the samples prepared under autoclave are wider, while the samples prepared under microwave are narrower, and for the samples prepared under oil-bath are sharper. The samples prepared in the autoclave have a more amorphous nature than the samples prepared in the oil bath and microwave.

The samples prepared under autoclave and microwave according to FESEM data have a more uniform texture than the sample prepared in oil-bath. The functionalized samples have greater average particle sizes and broadened particle size distributions compared to fullerene soot. Like fullerene soot, no exothermic peak is observed in the DSC thermogram of the sample prepared in the absence of 4-nitrophenylboronic acid. For the samples prepared in the presence of 4-nitrophenylboronic acid, an exothermic peak assigned to the decomposition of energetic groups is observed. The potentially energetic solid containing 4-nitrophenoxy groups with high thermal stability is produced in the absence of fullerene soot. The oxygen content in this sample is greater than the nitrogen, suggesting this sample contains higher ether linkages. The samples prepared in the longer reaction times and the higher temperatures have more energetic properties. The sample prepared in the presence of a catalyst in an oil bath has higher nitrogen content and better energetic performance among others. These findings may be helpful for the development of novel energetic compositions from carbon nanomaterials.

10.57647/ijc.2026.1601.06

Acknowledgments

This Article is dedicated to my newborn son, "Abtin Zamani" (birthday: 2 Feb. 2025). Also, the authors thank Dr. S. Ahmad Nabavi (Damghan University) for providing centrifuge service and the research committee of Damghan University.

Supporting Information
Supplementary material (Figures S1-S6) is available in the online version of this article.

Author contributions
Fatemeh Sadat Hosseini: Investigation, Formal analysis, Resources, Data Curation, Visualization.
Mehdi Zamani: Conceptualization, Methodology, Validation, Formal analysis, Resources, Data Curation, Writing - Original Draft, Writing - Review & Editing, Visualization, Supervision, Project administration.

Funding
None

Disclosure Statement
None of the authors has a conflict of interest to disclose.

Data availability statement
All data generated or analyzed during this study are included in this published article.

References

[1] Q.L. Yan, M. Gozin, F.Q. Zhao, A. Cohen, S.P. Pang, Nanoscale **8** (2016) 4799-4851. https://doi.org/ 10.1039/C5NR07855E

[2] B. Duan, J. Li, H. Mo, X. Lu, M. Xu, B. Wang, N. Liu, Molecules **26** (2021) 5650. https://doi.org/10.3390/molecules26185650

[3] S. Sriramrao, P. Raman, A. Dhas, S. Banerjee, Energ. Mater. Front. **5** (2024) 47-51. https://doi.org/10.1016/j.enmf.2024.02.001

[4] Z. Yang, H. Qi, J. Bo, P. Rufang, Chin. J. Explos. Propellants **45** (2022) 770. https://doi.org/10.14077/j.issn.1007-7812.202208009

[5] J. Anderson, D. Fitzgerald, In: 32nd Joint Propulsion Conference and Exhibit, 1996, 3211. https://doi.org/ 10.2514/6.1996-3211

[6] X. Han, T.F. Wang, Z.K. Lin, D.L. Han, S.F. Li, F.Q. Zhao, L.Y. Zhang, Def. Sci. J. **59** (2009) 284-293. https://doi.org/ 10.14429/dsj.59.1522

[7] G. Fan, L. Shufen, J. Energ. Mater. **21** (2003) 33-41. https://doi.org/ 10.1080/07370650305586

[8] S. Li, D. He, W. Shan, F. Zhao, S. Li, J. Propul. Technol. **18** (1997) 79-83.

[9] F. Zhao, S. Li, W. Shan, S. Li, J. Propul. Technol. **21** (2000) 72-76.

[10] X. Han, Y.L. Sun, T.F. Wang, Z.K. Lin, S.F. Li, F.Q. Zhao, Z.R. Liu, J.H. Yi, X.N. Ren, J. Therm. Anal. Calorim. **91** (2008) 551-557. https://doi.org/ 10.1007/s10973-007-8290-6

[11] S. Li, X. Han, Y. Sun, T. Wang, F. Zhao, In: 41st AIAA/ASME/SAE/ASEE Joint Propulsion Conference & Exhibit, 2005, 4473. https://doi.org/10.2514/6.2005-4473

[12] B.E. Greiner, R.A. Frederick Jr, M.D. Moser, J. Propul. Power **19** (2003) 713-715. https://doi.org/10.2514/2.6161

[13] H.J. Guan, R.F. Peng, B. Jin, H. Liang, F.Q. Zhao, X.B. Bu, W.J. Han, S.J. Chu, Bull. Korean Chem. Soc. **35** (2014) 2257-2262. https://doi.org/10.5012/bkcs.2014.35.8.2257

[14] H.J. Guan, B., Jin, R.F., Peng, F.Q., Zhao, W.J., Han, B.L. Chen, S.J., Chu, Acta Armamentarii **35** (2014) 1756. https://doi.org/10.3969/j.issn.1000-1093.2014.11.005

[15] V.V. Chaban, E.E. Fileti, O.V. Prezhdo, J. Phys. Chem. Lett. **6** (2015) 913-917. https://doi.org/10.1021/acs.jpclett.5b00120

[16] Y. Zhao, Z. Chai, S. Ye, Y. Xiao, Q. Zhang, B. Jin, R. Peng, Thermochim. Acta **663** (2018) 110-117. https://doi.org/10.1016/j.tca.2018.03.016

[17] M. Manafi Moghadam, M. Zamani, S.A. Pourmousavi, J. Phys. Chem. Solids **154** (2021) 110101. https://doi.org/10.1016/j.jpcs.2021.110101

[18] M. Manafi Moghadam, M. Zamani, Int. J. Quantum Chem. **121** (2021) e26504. https://doi.org/10.1002/qua.26504

[19] J.T. Abrahamson, C. Song, J.H. Hu, J.M. Forman, S.G. Mahajan, N. Nair, W. Choi, E.J. Lee, M.S. Strano, Chem. Mater. **23** (2011) 4557-4562. https://doi.org/10.1021/cm201947y

[20] S. Sarvarian, M. Zamani, Struct. Chem. **32** (2021) 1205-1217. https://doi.org/10.1007/s11224-020-01703-9

[21] Z. Shareh, M. Zamani, Fullerenes, Nanotubes Carbon Nanostruct. **31** (2023) 523-537. https://doi.org/10.1080/1536383X.2023.2187786

[22] F.S. Hosseini, M. Zamani, Fullerenes, Nanotubes Carbon Nanostruct. **33** (2025) 142-163. https://doi.org/10.1080/1536383X.2024.2398799

[23] M. Manafi Moghadam, M. Zamani, Comput. Theor. Chem. **1198** (2021) 113185. https://doi.org/10.1016/j.comptc.2021.113185

[24] S. Sarvarian, M. Zamani, S.A. Pourmousavi, J. Nanostruct. **11** (2021) 252-268. https://doi.org/10.22052/JNS.2021.02.006

[25] M. Korivand, M. Zamani, J. Solid State Chem. **294** (2021) 121851. https://doi.org/10.1016/j.jssc.2020.121851

[26] Z. Shareh, M. Zamani, Compos. Interfaces **30** (2023) 1173-1200. https://doi.org/10.1080/09276440.2023.2200600

[27] Z. Shareh, M. Zamani, Fullerenes, Nanotubes Carbon Nanostruct. **32** (2024) 192-206. https://doi.org/ 10.1080/1536383X.2023.2270090

[28] D. G. Hall, Chem. Soc. Rev. **48** (2019) 3475-3496. https://doi.org/10.1039/C9CS00191C

[29] M. Sheng, D. Frurip, D. Gorman, J. Loss Prev. Process Ind. **38** (2015) 114-118. https://doi.org/10.1016/j.jlp.2015.09.004

[30] N. Oger, E. Le Grognec, F.X. Felpin, Org. Chem. Front. **2** (2015) 590-614. https://doi.org/10.1039/C5QO00037H

[31] C. Cougnon, F. Gohier, D. Bélanger, J. Mauzeroll, Angew. Chem. **121** (2009) 4066-4068. https://doi.org/10.1002/ange.200900498

[32] 4-Nitrophenylboronic acid safety data sheet, Sigma-Aldrich Chemie GmbH. 2022. https://www.sigmaaldrich.com/DE/en/sds/aldrich/673854 (Accessed: 09.06.2024).

[33] C.N. McEwen, R.G. McKay, B.S. Larsen, J. Am. Chem. Soc. **114** (1992) 4412-4414. https://doi.org/10.1021/ja00037a064

[34] B.C. Yadav, R. Kumar, Int. J. Nanotechnol. Appl. **2** (2008) 15-24. https://www.academia.edu/download/44397281/Structure_properties_and_applications_of20160404-18129-nfful8.pdf (Accessed: October 2023)

[35] X. Yang, A. Ebrahimi, J. Li, Q. Cui, Int. J. Nanomed. 9 (2014) 77-92. https://doi.org/10.2147/IJN.S52829

[36] E.B. Zeynalov, N.S. Allen, N.I. Salmanova, Polym. Degrad. Stab. **94** (2009) 1183-1189. https://doi.org/10.1016/j.polymdegradstab.2009.04.027

[37] K. Kokubo, S. Yamakura, Y. Nakamura, H. Ueno, T. Oshima, Fullerenes, Nanotubes Carbon Nanostruct. **22** (2014) 250-261. https://doi.org/10.1080/1536383X.2013.812637

[38] Z. Markovic, V. Trajkovic, Biomaterials **29** (2008) 3561-3573. https://doi.org/10.1016/j.biomaterials.2008.05.005

[39] M.D. Tzirakis, M. Orfanopoulos, Chem. Rev. **113** (2013) 5262-5321. https://doi.org/10.1021/cr300475r

[40] P. Bhakta, B. Barthunia, J. Indian Acad. Oral Med. Radiol. **32** (2020) 159-163. https://doi.org/10.4103/jiaomr.jiaomr_191_19

[41] E. Carella, M. Ghiazza, M. Alfè, E. Gazzano, D. Ghigo, V. Gargiulo, A. Ciajolo, B. Fubini, I. Fenoglio, BioNanoScience **3** (2013) 112-122. https://doi.org/10.1007/s12668-013-0077-6

[42] I.V. Mikheev, M.M. Sozarukova, D.Y. Izmailov, I.E. Kareev, E.V. Proskurnina, M.A. Proskurnin, Int. J. Mol. Sci. **22** (2021) 5838. https://doi.org/10.3390/ijms22115838

[43] R. Czochara, J. Kusio, M. Symonowicz, G. Litwinienko, Ind. Eng. Chem. Res. **55** (2016) 9887-9894. https://doi.org/10.1021/acs.iecr.6b02564

[44] W. Zhu, D.E. Miser, W.G. Chan, M.R. Hajaligol, Carbon **42** (2004) 1463-1471. https://doi.org/10.1016/j.carbon.2004.01.076

[45] L.J. Dunne, A.K. Sarkar, H.W. Kroto, J. Munn, P. Kathirgamanathan, U. Heinen, J. Fernandez, J. Hare, D.G. Reid, A.D. Clark, J. Phys. Condens. Matter **8** (1996) 2127. https://doi.org/10.1088/0953-8984/8/13/005

[46] D.I. Bugaenko, A.A. Volkov, A.V. Karchava, M.A. Yurovskaya, Russ. Chem. Rev. **90** (2021) 116. https://doi.org/10.1070/RCR4959

[47] N. Kvasovs, V. Gevorgyan, Chem. Soc. Rev. **50** (2021) 2244-2259. https://doi.org/10.1039/D0CS00589D

[48] G. Yan, M. Yang, X. Wu, Org. Biomol. Chem. **11** (2013) 7999-8008. https://doi.org/ 10.1039/C3OB41851K

[49] S.D. Yang, C.L. Sun, Z. Fang, B.J. Li, Y.Z. Li, Z.J. Shi, Angew. Chem., Int. Ed. **47** (2008) 1473-1476. https://doi.org/10.1002/anie.200704619

[50] N. Miyaura, in: L.S. Liebeskind (Ed.), Advances in Metal-Organic Chemistry, Elsevier **6** (1998) 187-243. https://doi.org/10.1016/S1045-0688(98)80007-5

[51] X. Guan, H. Zhu, T.G. Driver, ACS Catal. **11** (2021) 12417-12422. https://doi.org/10.1021/acscatal.1c03113

[52] F. Behmagham, S.B. Azimi, M. Ubaid, A.T. Abd Ali, A.H. Adhab, M.H. Sami, S. Soleimani-Amiri, E. Vessally, RSC Adv. **13** (2023) 33390-33402. https://doi.org/10.1039/D3RA05100E

[53] T. Sakaguchi, K. Fukuoka, T. Matsuki, M. Kawase, A. Tazawa, Y. Uozumi, Y. Matsumura, O. Shimomura, A. Ohtaka, Synlett. **36** (2025) 161-165. https://doi.org/10.1055/a-2315-8369

[54] M. Patel, D. Bhavyesh, N. Kumar, H. Bhukya, B.Z. Dholakiya, T. Naveen, Asian J. Org. Chem. **13** (2024). e202400064. https://doi.org/10.1002/ajoc.202400064

[55] J.S. Tang, Y.X. Xie, Z.Q. Wang, J.H. Li, Synthesis **2011** (2011) 2789-2795. https://doi.org/10.1055/s-0030-1260126

[56] J. Zhang, J. Chen, J. Ding, M. Liu, H. Wu, Tetrahedron **67** (2011) 9347-9351. https://doi.org/10.1016/j.tet.2011.09.135

[57] R.L. McLaren, C.J. Laycock, D.J. Morgan, G.R. Owen, New J. Chem. **44** (2020) 19144-19154. https://doi.org/10.1039/D0NJ04187D

[58] Ü. Çalışır, B. Çiçek, M. Doğan, Fullerenes, Nanotubes Carbon Nanostruct. **29** (2021) 899-906. https://doi.org/10.1080/1536383X.2021.1913727

[59] K.A. Kurnia, W. Setyaningsih, N. Darmawan, B. Yuliarto, J. Mol. Liq. **326** (2021) 115321. https://doi.org/10.1016/j.molliq.2021.115321

[60] R4-Nitrophenylboronic acid application, Sigma-Aldrich Chemie GmbH. 2022. https://www.sigmaaldrich.com/DE/en/product/aldrich/673854 (Accessed: 09.06.2024).

[61] J. Huang, F. Ding, P. Rojsitthisak, F.S. He, J. Wu, Org. Chem. Front. **7** (2020) 2873-2898. https://doi.org/10.1039/D0QO00563K

[62] L. Hao, G. Ding, D.A. Deming, Q. Zhang, Eur. J. Org. Chem. **2019** (2019) 7307-7321. https://doi.org/10.1002/ejoc.201901303

[63] K. Inamoto, K. Nozawa, M. Yonemoto, Y. Kondo, Chem. Commun. **47** (2011) 11775-11777. https://doi.org/10.1039/C1CC14974A

[64] W. Yin, X. Pan, W. Leng, J. Chen, H. He, Green Chem. **21** (2019) 4614-4618. https://doi.org/10.1039/C9GC01965K

[65] R.N. Dhital, H. Sakurai, Asian J. Org. Chem. **3** (2014) 668-684. https://doi.org/10.1002/ajoc.201300283

[66] Y. Ding, L. Fu, X. Peng, M. Lei, C. Wang, J. Jiang, Chem. Eng. J. **427** (2022) 131776. https://doi.org/10.1016/j.cej.2021.131776

[67] C.J. Liang, C.J. Bruell, M.C. Marley, K.L. Sperry, Soil Sediment Contam.: Int. J. **12** (2003) 207-228. https://doi.org/10.1080/713610970

[68] D.D. Sun, X.X. Yan, W.P. Xue, Adv. Mater. Res. **610** (2012) 1209-1212. https://doi.org/10.4028/www.scientific.net/AMR.610-613.1209

[69] D.N. Mai, R.D. Baxter, Top. Catal. **60** (2017) 580-588. https://doi.org/10.1007/s11244-017-0734-z

[70] Chemistry of Boronic Esters, https://www.aablocks.com/node/31 (Accessed: October 2023)

[71] S. Pillitteri, P. Ranjan, E.V. Van der Eycken, U.K. Sharma, Adv. Synth. Catal. **364** (2022) 1643-1665. https://doi.org/10.1002/adsc.202200204

[72] Q. Wang, Y. Mei, R. Zhou, S. Komarneni, J. Ma, Colloids Surf., A **648** (2022) 129315. https://doi.org/10.1016/j.colsurfa.2022.129315

[73] C.A. Contreras-Celedón, L. Chacón-García, N.J. Lira-Corral, J. Chem. **2014** (2014) 569572. https://doi.org/10.1155/2014/569572

[74] M. Gohain, M. du Plessis, J.H. van Tonder, B.C. Bezuidenhoudt, Tetrahedron Lett. **55** (2014) 2082-2084. https://doi.org/10.1016/j.tetlet.2014.02.048

[75] C. McCarthy, N. Losada-Garcia, J.M. Palomo, Chemistry Select **5** (2020) 7492-7496. https://doi.org/10.1002/slct.202002110

[76] V. Sadhasivam, M. Harikrishnan, G. Elamathi, R. Balasaravanan, S. Murugesan, A. Siva, New J. Chem. **44** (2020) 6222-6231. https://doi.org/10.1039/C9NJ05759E

[77] I. Kumar, R. Sharma, R. Kumar, R. Kumar, U. Sharma, Adv. Synth. Catal. **360** (2018) 2013-2019. https://doi.org/10.1002/adsc.201701573

[78] E. Tsui, H. Wang, R.R. Knowles, Chem. Sci. **11** (2020) 11124-11141. https://doi.org/10.1039/D0SC04542J

[79] Q. Mei, H. Cao, D. Han, M. Li, S. Yao, J. Xie, J. Zhan, Q. Zhang, W. Wang, M. He, J. Hazard. Mater. **389** (2020) 121901. https://doi.org/10.1016/j.jhazmat.2019.121901

[80] Y. Ji, Y. Shi, Y. Yang, P. Yang, L. Wang, J. Lu, J. Li, L. Zhou, C. Ferronato, J.M. Chovelon, J. Hazard. Mater. **361** (2019) 152-161. https://doi.org/10.1016/j.jhazmat.2018.08.083

[81] G. Ghigo, A. Maranzana, G. Tonachini, C.M. Zicovich-Wilson, M. Causà, J. Phys. Chem. B **108** (2004) 3215-3223. https://doi.org/10.1021/jp037011+

[82] S. Antusch, M. Dienwiebel, E. Nold, P. Albers, U. Spicher, M. Scherge, Wear **269** (2010) 1-12. https://doi.org/10.1016/j.wear.2010.02.028

[83] E. Destandau, T. Michel, C. Elfakir, in: M.A. Rostagno, J.M. Prado (Eds.), Natural Product Extraction: Principles and Applications, The Royal Society of Chemistry, 2013, pp. 113-156. https://doi.org/10.1039/9781849737579-00113

[84] A. Kumar, Y. Kuang, Z. Liang, X. Sun, Mater. Today Nano **11** (2020) 100076. https://doi.org/10.1016/j.mtnano.2020.100076

[85] F.A. Bassyouni, S.M. Abu-Bakr, M.A. Rehim, Res. Chem. Intermed. **38** (2012) 283-322. https://doi.org/10.1007/s11164-011-0348-1

[86] S. Kobayashi, in: S. Kobayashi, K. Müllen (Eds.), Encyclopedia of Polymeric Nanomaterials, Springer, Berlin, Heidelberg, 2014, pp. 1-7. https://doi.org/10.1007/978-3-642-36199-9_416-1

[87] G. Wypych, in: G. Wypych (Ed.), Handbook of Polymers, ChemTec Publishing, Toronto, 2016, pp. 522-525. https://doi.org/10.1016/B978-1-895198-92-8.50162-2

[88] Y. Shimoyama, Y. Nakajima, ChemSusChem **16** (2023) e202300684. https://doi.org/10.1002/cssc.202300684

[89] M. Dmitrenko, A. Chepeleva, V. Liamin, A. Mazur, K. Semenov, N. Solovyev, A. Penkova, Polymers **14** (2022) 691. https://doi.org/10.3390/polym14040691

[90] S.Y. Lee, S.H. Mun, J.H. Jin, Y.K. Hong, Elastomers Compos. **46** (2011) 257-261. https://doi.org/10.7473/EC.2011.46.3.257

[91] N.T. Rebeck, Y. Li, D.M. Knauss, J. Polym. Sci., Part B: Polym. Phys. **51** (2013) 1770-1778. https://doi.org/10.1002/polb.23245

[92] H. Cong, B. Yu, H. Yuan, C. Tian, S. Yang, in: V. Mittal (Ed.), Manufacturing of Nanocomposites with Engineering Plastics, Woodhead Publishing, 2015, pp. 199-224. https://doi.org/10.1016/B978-1-78242-308-9.00009-4

[93] Y. Hu, G. Yu, C. Xing, S. Liu, C. Wei, H. Liu, J. Jiang, X. Li, ChemCatChem **13** (2021) 4591-4601. https://doi.org/10.1002/cctc.202101016

[94] H. Behniafar, S. Khosravi-borna, Polym. Int. **58** (2009) 1299-1307. https://doi.org/10.1002/pi.2663

[95] C.L. Chung, T.W. Tzu, S.H. Hsiao, J. Polym. Res. **13** (2006) 495-506. https://doi.org/10.1007/s10965-006-9072-8

[96] B. Rai, A. Kumar Patel, J.M. Keller, R. Bajpai, Int. J. Sci. Res. Dev. **4** (2016) 1197-1200.

[97] S. Kaur, P. Kumar, R. Thangaraj, Polym. Bull. **70** (2013) 2269-2276.
https://doi.org/10.1007/s00289-013-0948-6

[98] M.A. Semsarzadeh, A. Sh Dadkhah, A. Sabzevari, Polym. Polym. Compos. **30** (2022) 09673911221104678.
https://doi.org/10.1177/09673911221104678

[99] U.R. Nair, S.N. Asthana, A.S. Rao, B.R. Gandhe, Def. Sci. J. **60** (2010) 137.
https://doi.org/10.14429/dsj.60.327

[100] G. Ćirić-Marjanović, I. Pašti, S. Mentus, Prog. Mater. Sci. **69** (2015) 61-182.
https://doi.org/10.1016/j.pmatsci.2014.08.002

[101] K.N. Wood, R. O'Hayre, S. Pylypenko, Energy Environ. Sci. **7** (2014) 1212-1249.
https://doi.org/10.1039/C3EE44078H

[102] O.Y. Podyacheva, Z.R. Ismagilov, Catal. Today **249** (2015) 12-22.
https://doi.org/10.1016/j.cattod.2014.10.033

[103] Z.H. Yang, H.Q. Wu, Mater. Lett. **50** (2001) 108-114.
https://doi.org/10.1016/S0167-577X(00)00425-0

[104] M. Galizia, C. Daniel, G. Fasano, G. Guerra, G. Mensitieri, Macromol. **45** (2012) 3604-3615.
https://doi.org/10.1021/ma3000626

[105] M. Khayet, J.P.G. Villaluenga, M.P. Godino, J.I. Mengual, B. Seoane, K.C. Khulbe, T. Matsuura, J. Colloid Interface Sci. **278** (2004) 410-422.
https://doi.org/10.1016/j.jcis.2004.06.021

[106] H.A. Dabbagh, M. Zamani, Appl. Catal., A **404** (2011) 141-148.
https://doi.org/10.1016/j.apcata.2011.07.024

[107] J. Li, D. Liu, B. Li, J. Wang, S. Han, L. Liu, H. Wei, CrystEngComm **17** (2015) 520-525.
https://doi.org/10.1039/C4CE01632G

[108] P. Manjunathan, M. Kumar, S.R. Churipard, S. Sivasankaran, G.V. Shanbhag, S.P. Maradur, RSC Adv. **6** (2016) 82654-82660.
https://doi.org/10.1039/C6RA18609B

[109] C. Badeen, R. Turcotte, E. Hobenshield, S. Berretta, J. Hazard. Mater. **188** (2011) 52-57.
https://doi.org/10.1016/j.jhazmat.2011.01.063

[110] R.G. Ferrillo, A. Wilson, Thermochim. Acta **4** (1972) 273-281.
https://doi.org/10.1016/0040-6031(72)87011-4

[111] S. Weng, W. Feng, W. Wu, Z. Guo, L. Chen, W. Chen, Org. Process Res. Dev. **27** (2023) 1027-1035.
https://doi.org/10.1021/acs.oprd.2c00403

[112] Ł. Gutowski, S. Cudziło, Def. Technol. **17** (2021) 775-784.
https://doi.org/10.1016/j.dt.2020.05.008

[113] X. Zhang, H. Xiong, H. Yang, G. Cheng, Propellants, Explos., Pyrotech. **42** (2017) 942-946.
https://doi.org/10.1002/prep.201700030